

A PHOTOCHEMICAL STUDY OF NITROGEN DIOXIDE USING A PULSED RUBY LASER

by

David F. Hakala

5416

A Thesis Submitted to the Graduate

Faculty of Rensselaer Polytechnic Institute


in Partial Fulfillment of the

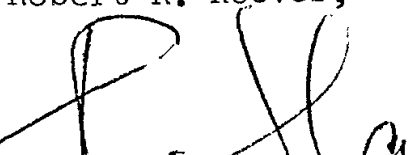
Requirements for the Degree of

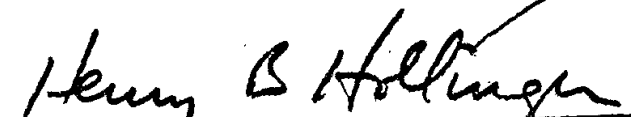
DOCTOR OF PHILOSOPHY

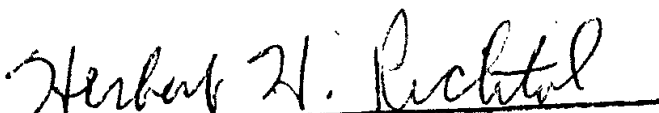
Major Subject: Photochemistry


Approved by the
Examining Committee:


Robert R. Reeves, Thesis Advisor


Paul Harteck, Member


Henry B. Hollinger, Member


Herbert H. Richtol, Member


Philip A. Casabella, Member

Rensselaer Polytechnic Institute
Troy, New York

May 1976

CONTENTS

	Page
LIST OF TABLES.....	v
LIST OF FIGURES.....	vi
ACKNOWLEDGEMENTS.....	viii
ABSTRACT.....	ix
1. INTRODUCTION.....	1
1.1 Fluorescence and Quenching of NO ₂	1
1.2 Multiphoton Dissociation Reactions.....	4
1.3 Multiphoton Fluorescence Studies.....	5
1.4 Intent of This Research.....	6
2. EXPERIMENTAL.....	8
2.1 Preparation of Samples and Materials.....	8
2.2 Experimental Apparatus.....	8
2.2.1 Laser System.....	8
2.2.2 Mass Spectrometer.....	12
2.2.3 Detection Electronics.....	12
2.2.4 System Arrangement.....	16
2.3 Experimental Procedure.....	18
2.3.1 Fluorescence and Quenching Studies.....	18
2.3.2 Multiphoton Photolysis Studies.....	20
2.3.3 Multiphoton Fluorescence Studies.....	22
3. RESULTS.....	24
3.1 Fluorescence and Quenching of NO ₂	24
3.1.1 Self-Quenching of NO ₂ at Low Pressures.....	24
3.1.2 Quenching by Foreign Gases.....	28
3.1.3 Self-Quenching of NO ₂ at High Pressures.....	28
3.2 Two-Photon Induced Dissociation of NO ₂	37
3.3 Multiphoton Induced Fluorescence of NO ₂	41

4. DISCUSSION.....	48
4.1 Fluorescence of NO ₂	48
4.1.1 Radiative Lifetime.....	49
4.1.2 Quenching of NO ₂ Fluorescence.....	54
4.1.3 Self-Quenching of NO ₂ at High Pressures.....	58
4.2 Two-Photon Dissociation of NO ₂	67
4.3 Multiphoton Induced Fluorescence.....	79
5. CONCLUSIONS.....	87
6. LITERATURE CITED.....	91
APPENDIX.....	95

LIST OF TABLES

		Page
Table 1	Laser Specifications.....	11
Table 2	Mass Spectrometer Sensitivities.....	13
Table 3	Photomultiplier Characteristics.....	15
Table 4	Quenching Rate Constants of NO ₂ * for a Series of Added Gases.....	32
Table 5	Isotope Effect on O ₂ Production.....	40
Table 6	Relative Ratio of 3hv to 2hv Processes in the Multiphoton Induced Emission.....	47
Table 7	Quenching Cross-Sections for NO ₂ * and Comparison with Other Values.....	56
Table 8	Theoretical Relationships between the Vibrational Deactivation Rate Constants.....	62
Table 9	Calculated Values for the Vibrational Deactivation Rate Constants.....	63
Table 10	Effective Absorption Coefficient Ratios Calculated from the Isotope Data.....	78
Table A1	Definition of Terms for the Two Photon Consecutive Absorption Calculations.....	99

LIST OF FIGURES

	Page
Figure 1	Graph of the $2\text{NO}_2 \rightleftharpoons \text{N}_2\text{O}_4$ Equilibrium..... 9
Figure 2	Photomultiplier Quantum Efficiencies..... 14
Figure 3	Filter Spectral Transmission Data..... 17
Figure 4	Fluorescence Observation Arrangement..... 19
Figure 5	Typical Decay Curve..... 25
Figure 6	Typical Semilog Plot to Obtain Lifetime..... 26
Figure 7	Stern-Volmer Plot for Pure NO_2 29
Figure 8	Stern-Volmer Plot for He, Ar, O_2 , CO_2 30
Figure 9	Stern-Volmer Plot for N_2 , CO, NO, N_2O 31
Figure 10	Sample Traces of Non-Exponential Decays..... 33
Figure 11	First Maximum Peak Intensity Versus Pressure of NO_2 35
Figure 12	Inverse Time to First Maximum Versus Pressure of NO_2 36
Figure 13	Formation of O_2 Versus Pressure of NO_2 38
Figure 14	Log of O_2 Formed Versus Log of Relative Laser Intensity... 39
Figure 15	Blue Fluorescence Intensity Versus Pressure of NO_2 42
Figure 16	Stern-Volmer Plot for the Blue Emission..... 43
Figure 17	Log of the Blue Fluorescence Intensity Versus Log of the Relative Laser Intensity for Various Pressures of NO_2 44
Figure 18	Order of the Blue Emission Intensity with Respect to Laser Intensity Versus the Inverse of the NO_2 Pressure..... 45
Figure 19	Approximate Potential Energy Diagram for the ON-O Bond.... 50
Figure 20	Parametric Dependence of the Quenching Cross-Section Using the Theory of Steinfeld and Selwyn..... 57
Figure 21	Calculated O_2 Production Curve for One Laser Pulse Using the Consecutive Absorption Model..... 73

Figure 22	Log of the Fraction of NO_2^* Molecules Forming O_2 Versus the Log of the Second Absorption Coefficient.....	75
Figure A1	Calculated Product per Laser Pulse Versus Delay Time for a Series of Absorber Pressures.....	100

ACKNOWLEDGEMENTS

The author wishes to thank his advisor, Dr. Robert R. Reeves, for the guidance and encouragement provided during the course of this research. Discussions with Dr. Paul Harteck were especially helpful and greatly appreciated. Also helpful were John Gerstmayr for initially working with the author on the ruby laser and Roger Waldron for his technical assistance.

Much gratitude is also expressed to my wife Kathy who typed this manuscript and, more importantly, put up with me and encouraged me during my educational career.

Financial support for my education and for my research was provided through a NASA grant, NGL 33-108-007, and is gratefully acknowledged.

A PHOTOCHEMICAL STUDY OF NITROGEN DIOXIDE USING A PULSED RUBY LASER

by

David F. Hakala

An Abstract of a Thesis Submitted to the Graduate

Faculty of Rensselaer Polytechnic Institute

in Partial Fulfillment of the

Requirements for the Degree of

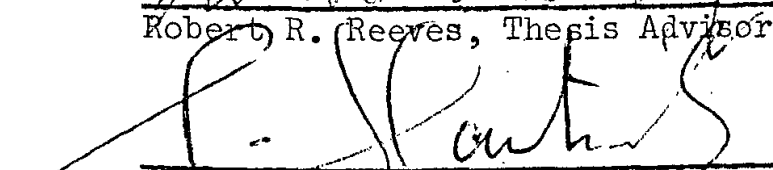
DOCTOR OF PHILOSOPHY

Major Subject: Photochemistry

The original of the complete thesis is on
file in the Rensselaer Polytechnic
Institute Library


Approved by the
Examining Committee:


Robert R. Reeves, Thesis Advisor


Paul Harteck, Member


Henry B. Hollinger, Member


Herbert H. Richtol, Member


Philip A. Casabella, Member

Rensselaer Polytechnic Institute
Troy, New York

May 1976

The processes, both physical and chemical, occurring as a result of the interaction between NO_2 and light from a high-power, pulsed ruby laser have been studied.

The absorption of a single quantum of light at a wavelength of $6943\overset{\circ}{\text{A}}$ raises the NO_2 molecule to an excited state (${}^2\text{B}_2$) where it can fluoresce, be electronically quenched to the ground state (${}^2\text{A}_1$), or vibrationally deactivate within the excited state manifold prior to either of the above two processes. These various primary processes were studied by time resolution of the emission using a filter-photomultiplier combination and storing the data by photographing the resulting oscilloscope trace.

At low pressures an exponential decay was observed and Stern-Volmer plots were used to determine the radiative lifetime and electronic self-quenching rate constant for NO_2 , as well as the electronic quenching rate constants for a series of added gases.

At higher pressures of NO_2 the decay was markedly non-exponential, emission maxima actually occurring. The data is consistent with a consecutive stepwise vibrational deactivation mechanism wherein the detection system is more sensitive to the radiation from intermediate states than to the initially formed excited state. Analysis of the data, using different theoretical models for vibrational deactivation to relate the rate constants to one another, gave values for the vibrational deactivation rate constant in the order of $4 \times 10^{-10} \text{ cm}^3/\text{part-sec}$. This effect was

observed only for addition of NO_2 and is probably a result of enhancement of the $V \rightarrow T$ transfer rate due to the chemical bond potential available to the $\text{NO}_2^*-\text{NO}_2$ pair. The vibrational deactivation rate constants for the other added gases must be much less than the corresponding electronic deactivation rate constants.

The dissociation of NO_2 by a two-step consecutive absorption process was also observed. The breaking of the ON-O bond followed by the reaction of the O atom with NO_2 leads to the production of molecular O_2 which was measured mass spectrometrically. An estimate of the second absorption coefficient on the order of $3.3 \text{ cm}^{-1} \text{ atm}^{-1}$ was made. An attempt was made to observe isotope-selective formation of O_2 , but results were inconsistent probably due to the temperature instability of the available ruby laser.

Multiphoton induced emission in the blue spectral region ($\sim 4,000\text{--}4,400\text{\AA}$) was observed at high pressures of NO_2 (~ 4 to 65 torr). The lifetime of the emission is compatible with an NO_2^* formed below the dissociation limit that quenches at an efficiency of about 10% the gas kinetic collision rate. The dependence of the emission intensity on laser intensity changes from third order at the lower pressures to a limiting value of two at the higher pressures. By considering the emission to be a sum of two and three photon processes it was shown that the two photon process was proportional to the square of the pressure and the three photon process to be linearly dependent on pressure.

These processes were interpreted as being two-photon consecutive absorptions with a deactivating step prior to the second

absorption. In the two-photon process the deactivating step is collisional, adding another order in the pressure dependence. In the three-photon process it is proposed that the deactivating step is an anti-Stokes Raman scattering of a laser photon off the NO_2^* intermediate. This maintains the pressure linearity and adds another order in laser intensity.

INTRODUCTION

1.1 Fluorescence and Quenching of NO₂

The fluorescence of NO₂ was first studied by Norrish as early as 1929 using steady state mercury arc illumination.¹ Subsequent examination by Baxter in 1930 of the fluorescence quenching of NO₂ by a series of added gases indicated that the excited state, NO₂^{*}, possessed either an unusually large collision cross-section or an unexpectedly long radiative lifetime.² About the same time, Heil estimated a 10 microsecond lifetime for the NO₂^{*} by measurement of the diffusion of NO₂^{*} from a narrow exciting beam; this fitting in with the model of a normal gas kinetic collision cross-section and long lifetime.³ In 1954 Neuberger and Duncan observed the NO₂^{*} decay directly using broadband flashlamp excitation and obtained a value of 44 microseconds for the radiative lifetime.⁴ An extensive study of the quenching of NO₂^{*} fluorescence excited by a series of mercury lines at 4047, 4358, 5461, and 5770 Å for a large number of added gases was performed by Myers, Silver, and Kaufman in 1965, and this was the last study of quenching of NO₂^{*} by other gases than NO₂ itself.⁵

Further research into the processes occurring in electronically excited NO₂ was motivated by the following facts. Firstly, the integrated absorption coefficient predicts a radiative lifetime that is approximately 100 to 200 times shorter than the experimentally observed lifetime.⁶ This is anomalous in view of the fact that usually the calculated lifetimes are longer than experimental ones due to the

occurrence of such processes as predissociation, intersystem crossing, and internal conversion.

Several authors have studied the variation of the NO_2^* radiative lifetime as a function of excitation wavelength.⁷⁻¹⁰ Kaufman, et al, observed no lifetime variation using a phase-shift technique, but their results are suspect due to the small size of their fluorescence cell, wall deactivation of the NO_2^* being a limiting factor.⁷ Sackett and Yardley, on the other hand, have observed significant wavelength variation using pulsed dye laser excitation and a large fluorescence cell designed to minimize wall quenching effects.⁹ The only other research performed on NO_2 at $6943\overset{\circ}{\text{A}}$ using a ruby laser (which is the longest wavelength used in any previous studied) was done by Calvert and co-workers and dealt with the fluorescence lifetime and self-quenching constant for NO_2 but did not include measurement of quenching constants of other gases.¹⁰ Also, the lifetime data showed a large limit of error for the $6943\overset{\circ}{\text{A}}$ measurement, which could potentially be improved.

A second motivation for the further research was that the absorption and fluorescence spectra of NO_2 show remarkable complexity for such a simple molecule; a more complete understanding of them being of fundamental importance.

Recent spectroscopic studies by Brand and Hardwick have established the (0,0,0) levels of $^2\text{B}_1$ and $^2\text{B}_2$ excited states as being at $14,743\text{ cm}^{-1}$ and $11,956\text{ cm}^{-1}$, respectively.^{11,12} Since the laser line at $6943\overset{\circ}{\text{A}}$ corresponds to $14,403\text{ cm}^{-1}$ and the work of

Brand and Hardwick indicates little or no absorption by the 2B_1 state at longer wavelengths, the laser will selectively excite the 2B_2 state and data on its lifetime and quenching behavior will shed more light on the nature of coupling among the electronic states of NO_2 .

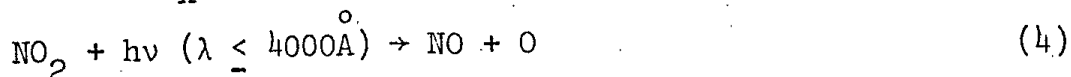
A final reason for this type work may be considered due to the importance of NO_2^* in atmospheric chemistry. The airglow which results from the NO and O recombination,



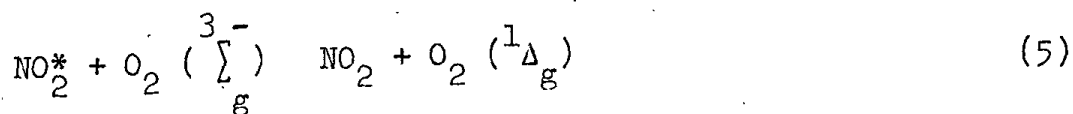
has been a subject of many kinetic and spectroscopic investigations,¹³⁻¹⁶ and is due to the emission of light by the chemically formed NO_2^* . Similar to the NO-O reaction is the bimolecular chemiluminescent reaction,



which can be used in a technique for the measurement of low ambient levels of O_3 in the atmosphere.¹⁷ Furthermore, the photodissociation by sunlight of NO_2 (which is present in the atmosphere to a large extent as a result of NO_x emissions from automotive exhaust),



is the initiating step in the photochemical smog cycle.¹⁸ More recently, studies have shown that the reaction,



proceeds with a fairly high efficiency.¹⁹ The $O_2 (^1\Delta_g)$ is known to be a fairly reactive species and readily oxidizes unsaturated hydrocarbons.²⁰ This reaction can extend the potentially smog-forming wavelengths towards the red, and accurate deactivation rate constants for NO_2^* formed at

lower excitation energies may be important in the modelling of the photochemical smog cycle.

1.2 Multiphoton Dissociation Reactions

Under the influence of a high intensity radiation field, nonlinear processes become increasingly more important. Limiting ourselves to two-photon interactions, there are two important and distinct processes that can occur.

In the first type of process, that of simultaneous two-photon dissociation, the first photon, $h\nu_1$, brings the molecule not to an energy level that is an eigenvalue of the time-independent Hamiltonian, but rather to a "virtual" state that is a superposition of the time-independent eigenfunctions. This "virtual" state can then absorb a second photon, $h\nu_2$, that brings the molecule to an energy level that is a time-independent eigenvalue.²¹ If this energy level happens to be in the dissociation continuum, or if the level can eventually lead to predissociation, then the molecule can obviously dissociate.

Examples of this type of process include the photo-initiated polymerization of styrene and of *p*-isopropylstyrene reported by Pao and Rentzepis,²² the dissociation of Cl_2 by a ruby laser initiating the $\text{H}_2\text{-Cl}_2$ explosion reported by Porter,²³ the dissociation of iodoform, CH_3I , leading to I_2 formation reported by Speiser and Kimel,²⁴ and more recently the dissociation of H_2O vapor leading to an OH radical which is readily detectable by resonance fluorescence reported by Wang and Davis.²⁵

The simultaneous process is characterized by very low primary product yields (at the laser intensities used), by the fact that the

product yield should show a squared dependence of the light intensity, and by the fact that no quenching effects should be observed except at extremely high pressures (since the "virtual" state is so short lived).

The second type of process is that of consecutive absorption of two photons wherein the initial photon brings the molecule to a real state of the system in a normal absorption. The excited state thus formed can fluoresce, undergo quenching or reaction; or it can absorb a second photon which brings the molecule to a dissociating state. The initial absorption step can be made very selective and this process has importance as a means of isotope separation.

Examples of this type of process include the photodissociation of phthalocyanine reported by Porter,²⁶ the dissociation of NH_3 reported by Letokhov,²⁷ the dissociation of BCl_3 reported by Rockwood,²⁸ and the dissociation of NO_2 as performed in this laboratory and initially reported by Gerstmayr, et al.²⁹

Consecutive absorption is characterized by much higher yields than for simultaneous absorption, by a dependence on light intensity that varies from first to second order subject to various molecular parameters and experimental conditions, and by a pressure dependent quenching since the intermediate excited state has a much longer lifetime in comparison with the "virtual" state.

1.3 Multiphoton Fluorescence Studies

Multiphoton fluorescence studies have generally dealt with systems excited by the simultaneous absorption process. One example of such a process is the work of Schlag and co-workers in obtaining

the two-photon excitation spectrum of benzene in the gas phase.³⁰ The excitation was to the first excited singlet state of benzene. The one-photon absorption is allowed and the two-photon absorption forbidden for the $S_0 \rightarrow S_1$ transition, but Herzberg-Teller coupling of the vibrational and electronic states will allow certain vibronically-induced two-photon absorptions to vibronic levels not accessible by direct one-photon excitation. The collision-free lifetimes for some of these vibronic levels were also measured and related to non-radiative transitions from the S_1 state.³¹

In another study Hänsch and co-workers observed Doppler-free two-photon absorption using the $1S \rightarrow 2S$ transition in atomic hydrogen.³ The dye laser beam at $4860\overset{\circ}{\text{\AA}}$ was frequency doubled by use of a lithium formate monohydrate crystal to $2430\overset{\circ}{\text{\AA}}$, which was focused into the cell, reflected and refocused to provide a standing wave field to cancel the Doppler-shift. Collisions induced the $2S \rightarrow 2P$ transition and the L_{α} line at $1215\overset{\circ}{\text{\AA}}$ served to monitor the two-photon absorption. Absorption from the $2S$ level was observed simultaneously using the dye laser fundamental at $4860\overset{\circ}{\text{\AA}}$ which coincided with the visible Balmer- β line.

1.4 Intent of This Research

The intent of the research performed was to study the fluorescence of NO_2 as excited by the pulsed ruby laser in order to obtain information on the collision-free lifetime of NO_2 and to obtain data on the quenching of NO_2 by a series of foreign gases,

as well as on the self-quenching of NO_2 at higher pressures, which can be used to study relaxation within the excited state.

The two-photon dissociation of NO_2 , observed by Gerstmayr was to be studied in greater detail, experiments including laser intensity variation to study the order of the process with respect to laser intensity, as well as photolysis of some isotopically substituted NO_2 to ascertain if an isotope effect could occur.

A search for multiphoton induced fluorescence in the NO_2 was to be carried out. Emission from the dissociating state reached by the consecutive two-photon absorption was possible, although unlikely due to its very short lifetime.

The data obtained from such a study are of potential importance and interest to atmospheric chemistry and physics, photochemical isotope separation processes, and the fundamental dynamics of excited states.

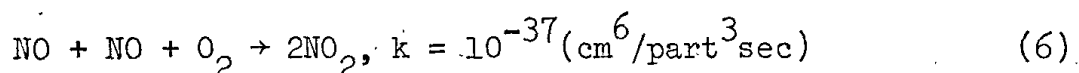
PART 2

EXPERIMENTAL

2.1 Preparation of Samples and Materials

For most of the experiments performed the gases used were obtained from the Matheson Company, East Rutherford, New Jersey, and generally used without further purification.

Clean nitrogen dioxide was prepared by the three body reaction of nitric oxide with oxygen,



where O_2 was present in excess. Passage of the reaction mixture through a liquid nitrogen trap (-196°C) froze down the NO_2 as solid N_2O_4 , while the majority of the excess O_2 was pumped away. Successive freeze-pump-thaw cycles (two to four) further removed any O_2 or N_2 entrained in the NO_2 . A final cycle using a dry ice-acetone bath (-77°C) removed any trace CO_2 . Mass spectral analysis of NO_2 or NO_2/Ar mixtures typically showed small background amounts of N_2 , O_2 , and H_2O .

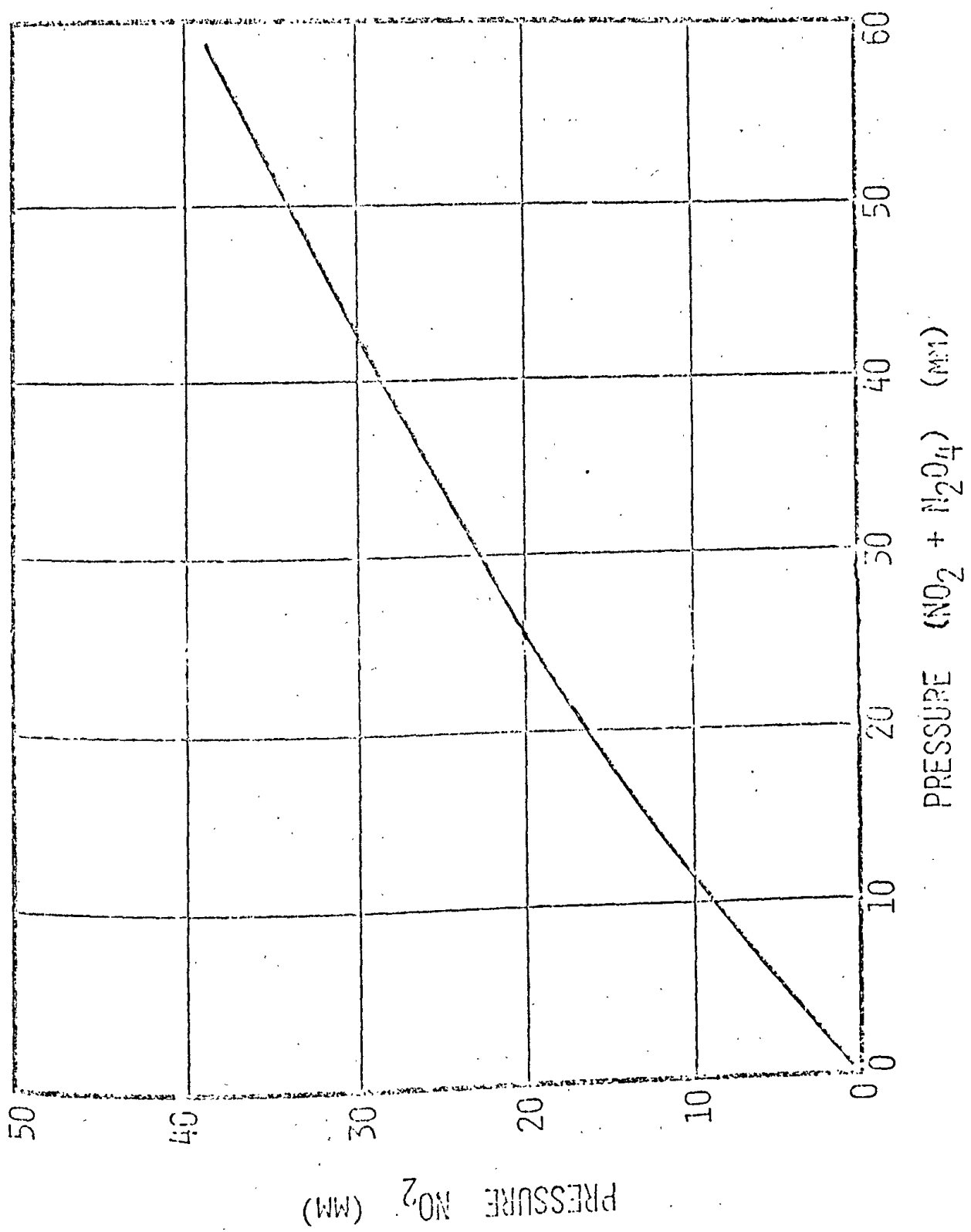
Partial pressures of NO_2 and N_2O_4 were calculated using the data of Harris and Churney.³³ A graph of P_{NO_2} vs $(P_{\text{NO}_2} + P_{\text{N}_2\text{O}_4})$ is shown in Figure 1.

2.2 Experimental Apparatus

2.2.1 Laser System

The laser system used in these studies was a Korad K-1 flashlamp-pumped ruby laser. The 9/16" by 4" ruby rod was Q-switched using an electro-optical Pöckels cell to obtain a single giant pulse.

Figure 1 Graph of the $2\text{NO}_2 \rightleftharpoons \text{N}_2\text{O}_4$ Equilibrium



The pulse duration as observed using either photomultiplier or photodiode detection systems was about 15 to 20 nanoseconds. The linewidth of the laser was specified as being 0.06\AA by the manufacturer. Laser specifications are summarized in Table I.

The pulse energy was about 2 joules as measured using the Korad KJ-2 calorimeter. The energy measurements are performed as in a typical calorimetric experiment. The entire energy of the laser pulse was absorbed by a liquid of known volume and heat capacity. A thermocouple measured the temperature rise and the output was calibrated by the manufacturer as being 15 microvolts per joule of incident energy. Five pulses were run and the average of these taken. The individual points never varied by more than 3% from the average.

The laser was fired no faster than once every two minutes to prevent damage to the ruby rod from overheating.

The temporal distribution of the laser pulse could be most easily monitored by using a filtered (CS-2-60) RCA 1P21 photomultiplier which was looking at the reflection of the scattered laser light off the ceiling, and displaying the output on a Tektronix 545A or 7904 oscilloscope.

The laser intensity was varied using attenuation of the beam by reflection off of flat Pyrex glass plates held at set angles in slotted aluminum channeling mounted on the optical rail. The plates were paired off to insure that the beam axis was not grossly changed by refraction. Different numbers of plates were used to obtain different attenuations. The apparatus was calibrated by measuring

Table I
Laser Specifications

Pulse Energy	2 joules
Pulsewidth	15-25 nanosec (Pöckels cell Q-switch)
Wavelength	$6943\overset{\circ}{\text{Å}}$
Linewidth	$0.06\overset{\circ}{\text{Å}}$
Beam Diameter	9/16 in.
Beam Divergence	4 milliradians

the change in transmission of a Spectra-Physics Helium-Neon laser.

This arrangement does not have the flexibility of varying the flashlamp discharge voltage, but is far more accurate, to within 1 to 2 percent in the values for the effective transmittance of the system.

2.2.2 Mass Spectrometer

The mass spectrometer used for analyses was a Consolidated Electrodynamics Corporation 21-130 cycloidal focusing instrument. The ionizing voltage was fixed at 70 electron volts and samples were run at either a 30 or 90 microamp filament emission depending on sample size. Representative relative and absolute sensitivities for gases of interest are given in Table 2.

For the photodissociation experiments the sensitivities for Ar, O₂, and N₂ are particularly important, and these were checked frequently when the experiments were in progress. An expansion volume, normally open, was closed off due to the small sample size when these experiments were run.

For isotopic work, the resolution of the mass spectrometer, $R = M/\Delta M = 250$, is low and precluded direct analysis of molecular ions at nominally the same mass such as $(O^{16})_2^+$ in the presence of large amounts of $(N^{14}O^{18})^+$.

2.2.3 Detection Electronics

For the infra-red studies an RCA C31000F photomultiplier with a Hewlett-Packard power supply at 2300 V was used. For the near ultraviolet-blue studies an RCA 8575 was used. Photomultiplier response curves are shown in Figure 2 and photomultiplier data are given in Table 3. Both photomultipliers were mounted on Ortec 265

Table 2

Mass Spectrometer Sensitivities*

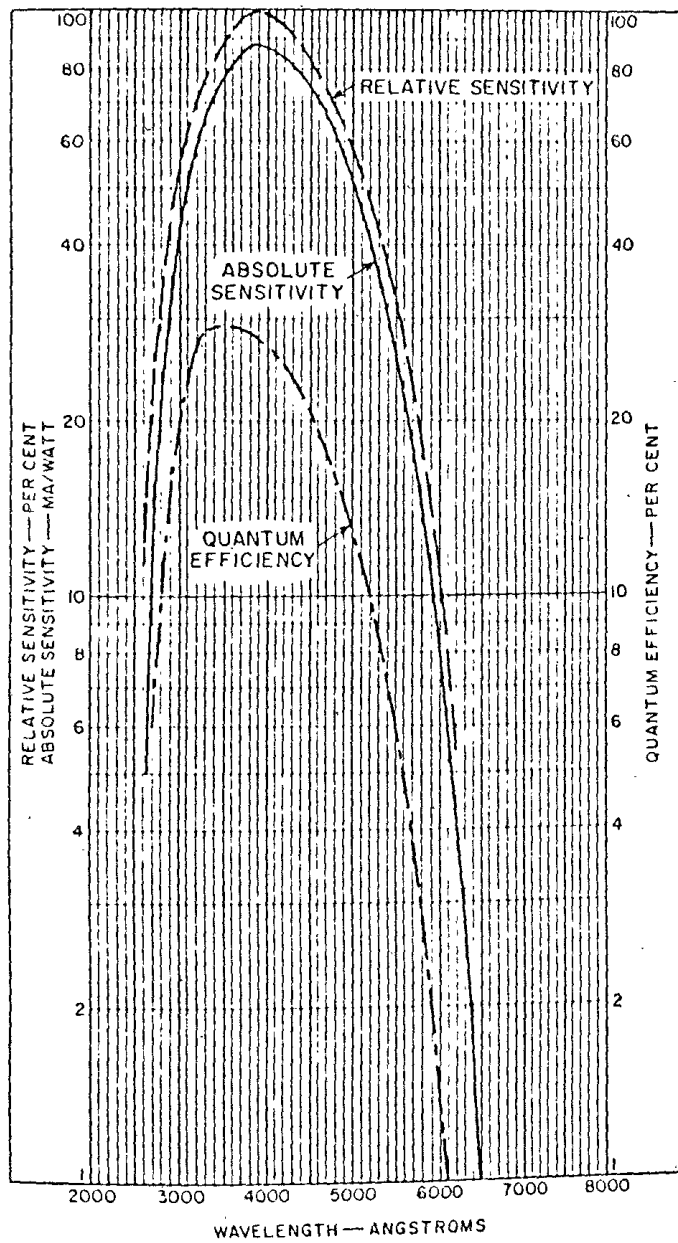
<u>Gas</u>	<u>m/e</u>	<u>Absolute Sens. (div/μ)</u>	<u>Relative Sens.</u>
He	4	10.77	0.288
N ₂	28	36.88	0.987
CO	28	35.95	0.963
NO	30	31.78	0.851
O ₂	32	27.86	0.746
Ar	40	37.35	1.000
CO ₂	44	31.96	0.856
N ₂ O	44	23.19	0.621
NO ₂	30**	29.10	0.779

* These were measured at an ionizing voltage of 70 ev and a filament current of 30 μ A.

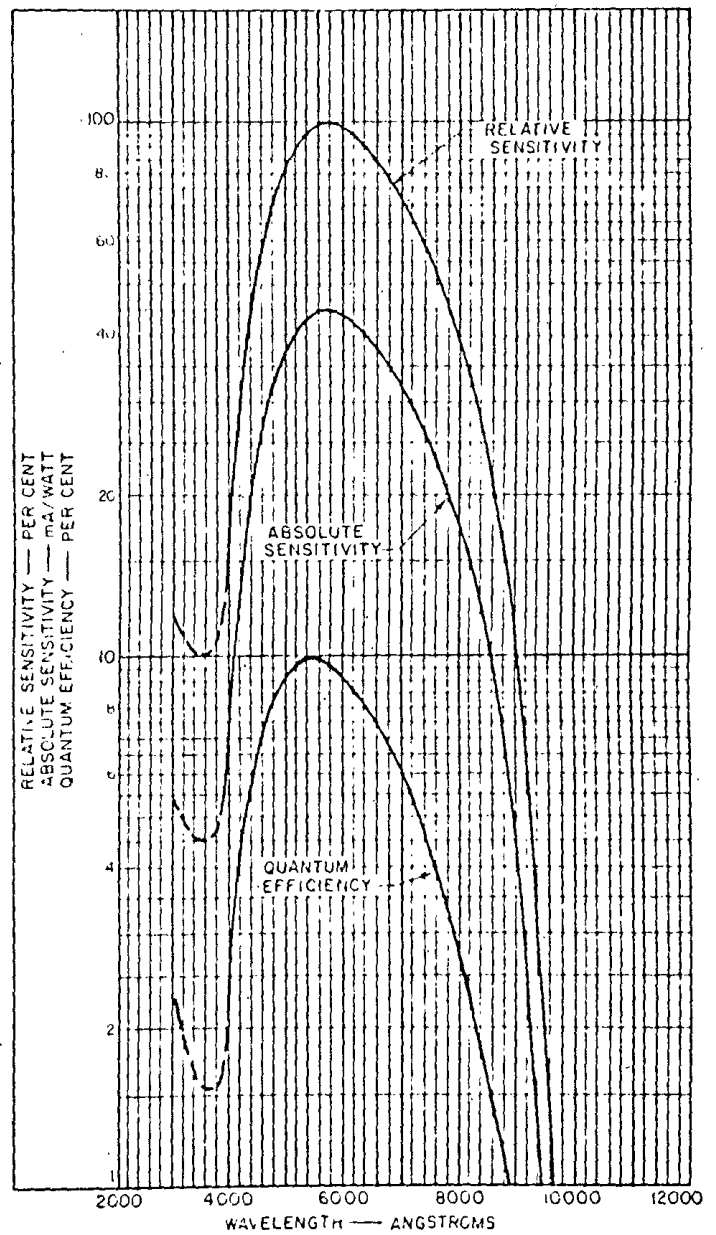
** Under the above conditions an extremely small m/e = 46 peak shows up, the fragmentation peak at m/e = 30 is therefore used for measurement.

Figure 2 Photomultiplier Quantum Efficiencies

Typical Spectral Response Characteristics



8575



C31000F

Table 3

Photomultiplier Characteristics

	<u>8575</u>	<u>C31000F</u>
Maximum Response λ	$3850\overset{\circ}{\text{A}}$	$5750\overset{\circ}{\text{A}}$
Cathode Type	Cs-K-Sb	Na-K-Cs-Sb
Maximum Anode to Cathode DC Supply Voltage	3000V	2500V
Current Amplification	$3.6 \times 10^{7(a)}$	$4 \times 10^{5(b)}$
Maximum Average Anode Current	0.2mA	1mA
Pulse Current (Saturation)	0.75A	0.5A

(a) For a DC Supply Voltage = 2500V

(b) For a DC Supply Voltage = 1500V

photomultiplier bases.

The photomultiplier outputs were connected to 50 Ω inputs on a Tektronix 7A19 amplifier of a 7904 oscilloscope.

The 7B18 time base was triggered externally by a pulse from a sync output of the Pöckels cell shutter electronics.

The resulting analog display was photographed using the Taktronix C-51 camera unit.

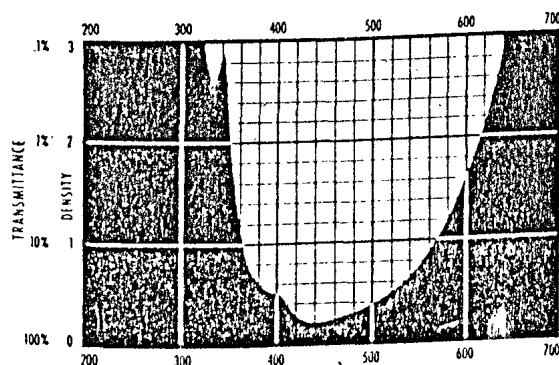
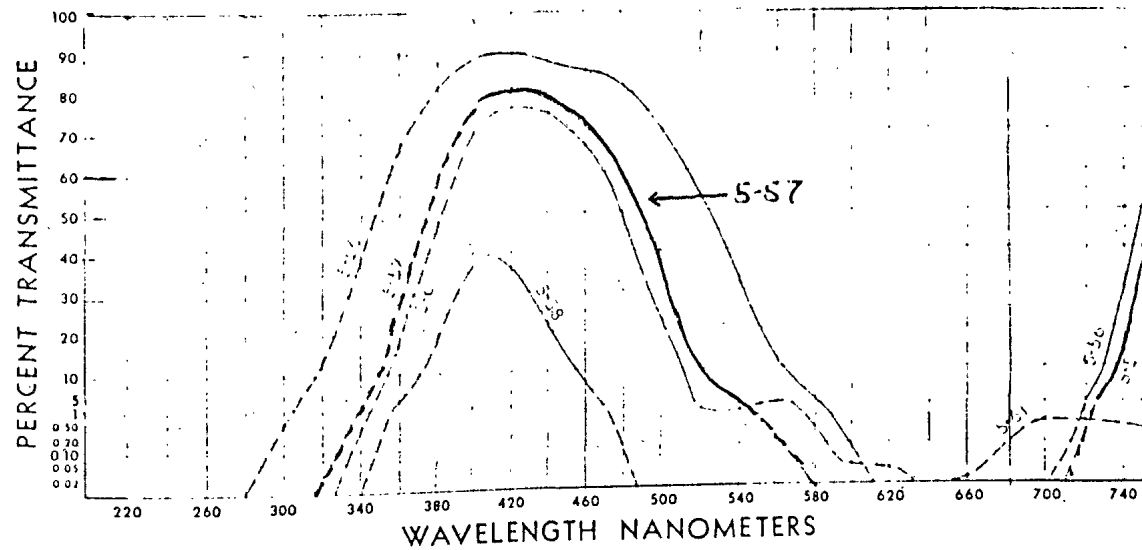
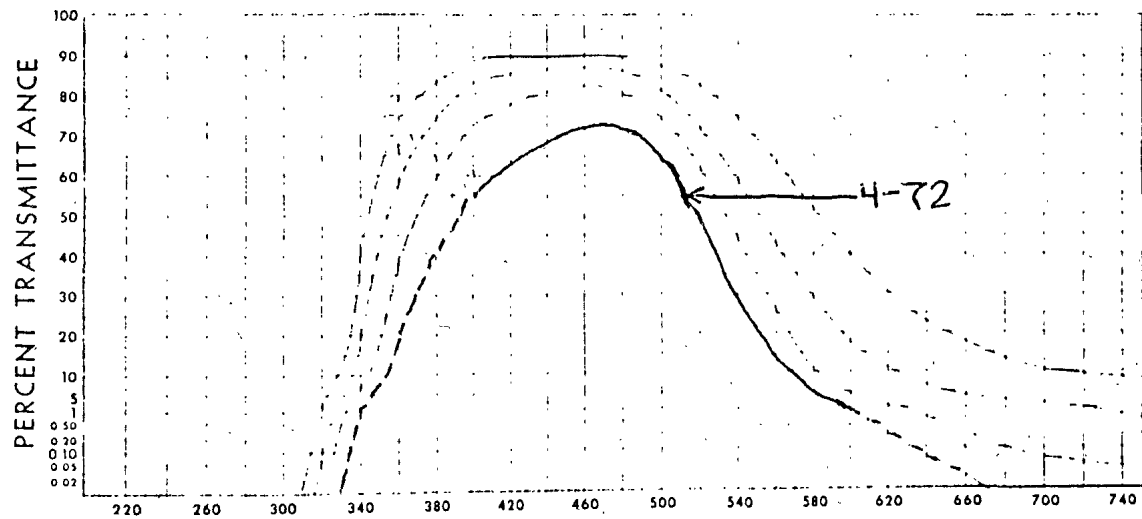
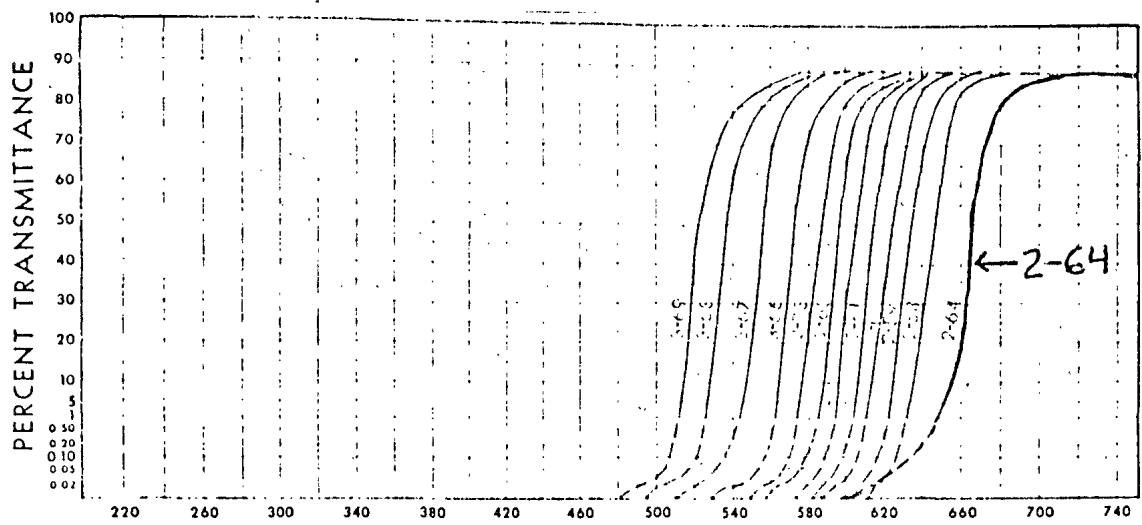
2.2.4 System Arrangement

In the photolysis experiments a 9.5 cm long optical cell was aligned with the laser beam axis on the optical rail. After the photolyses were performed the cell was taken to the mass spectrometer for analysis.

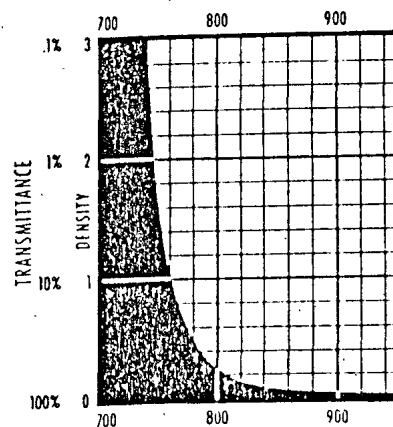
The fluorescence studies, both in the infrared and blue spectral regions, used the same general experimental arrangement. A 21.5 cm diameter spherical Pyrex bulb with Pyrex windows mounted on cylindrical glass sleeves was used as the fluorescence cell. The laser beam passed through these windows, and light emission was observed at right angles.

The primary or excitation filter used in the experiments was a Corning CS-2-64. The secondary or fluorescence filter combination used in the infrared studies consisted of two Corning filters CS5-57 and a Kodak Wratten 87 filter. The second filter combination used in the blue studies was two Corning CS4-72 filters, a Corning CS5-57 filter and a Kodak Wratten 38A filter. The transmission data for the appropriate filters is shown in Figure 3.

Figure 3 Filter Spectral Transmission Data



38A



The photomultiplier was located at a right angle to the laser beam and a mask limited the observation region in a manner that was designed to minimize the effects of NO_2^* deactivating by wall collision. A schematic of the fluorescence arrangement is shown in Figure 4.

Pressures in the flask were measured using a Decker Corporation differential pressure sensor with a full scale sensitivity of 10 volts corresponding to a pressure difference of 550 millitorr. The manufacturer's stated sensitivity agreed with that of a calibration by expansion using known volumes to within 1%.

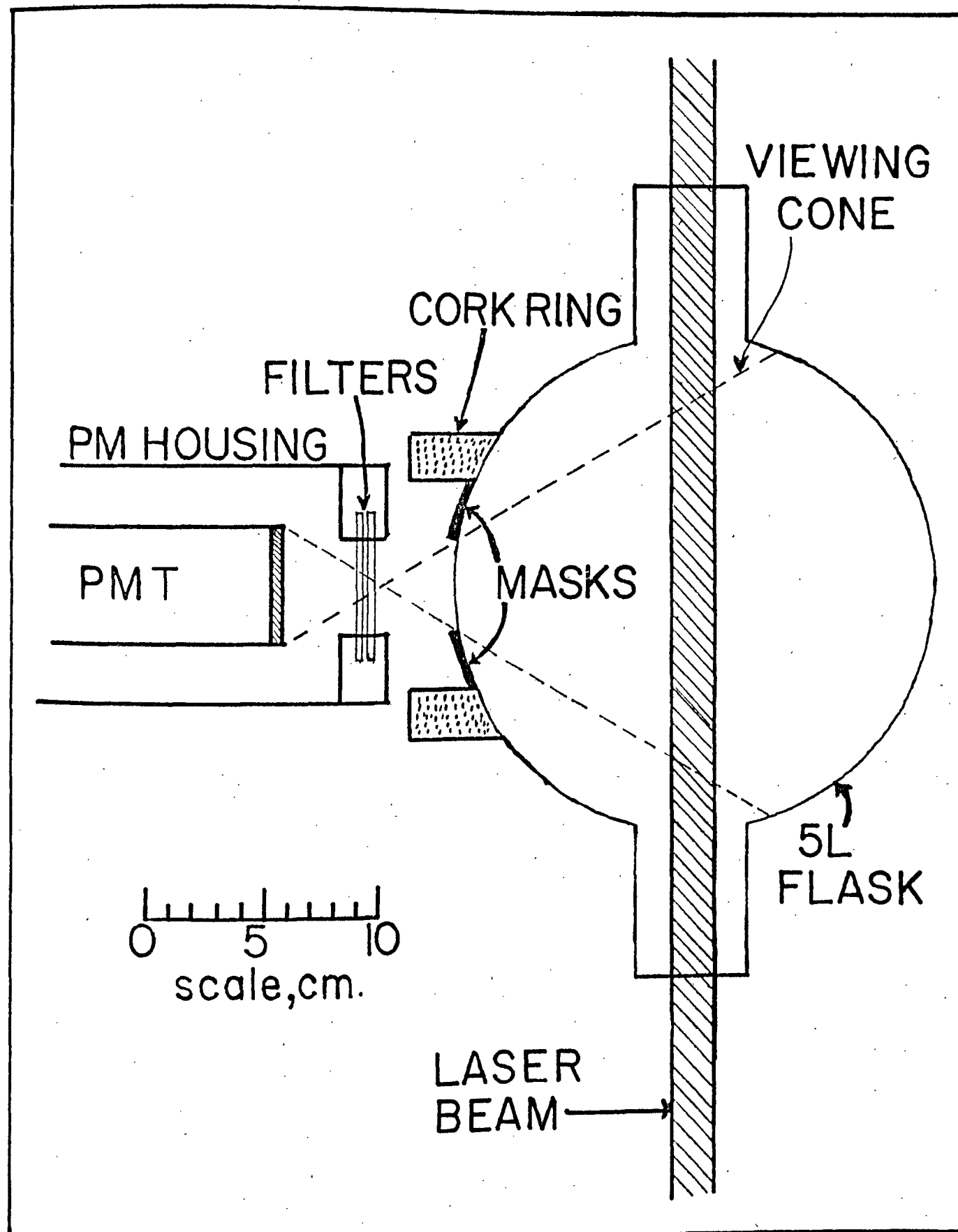
The vacuum system was all glass with Teflon and/or silicone grease stopcocks used to handle NO_2 ; all other stopcocks were greased with Apiezon N grease. With the liquid N_2 cold trap, mercury diffusion pump, and mechanical oil pump, the system would routinely pump to less than 10^{-4} torr, as measured by an NRC Alphatron pressure gauge.

2.3 Experimental Procedure

2.3.1 Fluorescence and Quenching Studies

The radiative lifetime and self-quenching constant for NO_2 was determined by adding the NO_2 incrementally to the evacuated fluorescence cell. The laser was fired, and the resulting oscilloscope trace was photographed. The oscilloscope trace was triggered using a timing output signal from the shutter control for the Pöckel cell Q-switch. The RCA C31000F photomultiplier was driven by a Hewlett-Packard high-voltage power supply with the PMT base anode held at -2300 V with respect to the photocathode. A trace of intensity versus time was obtained for each laser pulse.

Figure 4 Fluorescence Observation Arrangement



OBSERVATION ARRANGEMENT

The fluorescence data on pure NO_2 was taken at various pressures over a 3 to 500 millitorr range. From the low pressure data, values for the collision-free radiative lifetime and self-quenching rate constant could be extracted, as will be discussed later. The higher pressures give information on the collisional removal of energy from the electronically excited NO_2 .

For the quenching studies of foreign gases a fixed pressure of NO_2 of about 70 millitorr was placed in the evacuated fluorescence cell and the foreign gas being studied was added incrementally, the emission intensity being monitored as for the pure NO_2 experiments.

2.3.2 Multiphoton Photolysis Studies

The photolysis cell was 9.5 cm long with a volume of approximately 40 cm^3 . The laser was fired five times, once every two minutes, to obtain a data point. The low repetition rate is necessary to insure that the ruby rod cools sufficiently, after the flashlamp firing, in order to avoid cracking of the rod.

The O_2 formed was analyzed using the CEC 21-130 mass spectrometer. The sample was flowed through a U-tube at liquid nitrogen temperature before entering the mass spectrometer. All the NO_2 was frozen out on the walls. A known amount of argon was added to the NO_2 used in these experiments to provide a non-reactive, quantitative mass-spectrometer standard. The gas mixture was $2/3 (\text{NO}_2 + \text{N}_2\text{O}_4)$ and $1/3 \text{ Ar}$. The O_2 and Ar were measured without interference at $m/e = 32$ from the $^{14}\text{N}^{18}\text{O}^+$ peak which ordinarily would make impossible the measurement of small amounts of O_2 in NO_2 using a low resolution mass spectrometer. Back reaction of O_2 with

either NO or solid N_2O_3 was estimated to be negligible under the experimental conditions during the time period from the start of the photolysis to the end of the analysis (~ 20 minutes).

Laser intensity was varied by firing the ruby laser through flat Pyrex plates held at set angles in slotted aluminum channeling mounted on an optical rail. The plates were paired off at opposing but equal angles from vertical to maintain the beam direction and correct for offsets due to refraction on passing through a plate. This apparatus was calibrated using a Spectra-Physics continuous mode He-Ne laser, monitoring the transmitted intensity with a filtered RCA 1P21 photomultiplier. This arrangement allows one to make a \log (product) versus \log (laser intensity) plot and obtain the order of the process with respect to laser intensity from the slope.

Also attempted were some isotope effect experiments. A mixture of 51.3% argon and 48.7% ($\frac{2}{3} \text{N}^{16}\text{O}_2 + \frac{1}{3} \text{N}^{16}\text{O}^{18}\text{O}$) was made up. The O_2 production experiments were carried out as usual, but a test photolysis using sunlight for 25 minutes was also performed. This was done to insure a continuum photolysis to compare the calculated and experimental $\text{O}^{16}\text{O}^{18}/\text{O}_2^{16}$ ratios for random, non-selective excitation with the results obtained from laser excitation.

The results obtained will be discussed later, but it can be mentioned now that they were not reproducible to any great accuracy. Since it is known that the lasing wavelength can be changed from $6943\overset{\circ}{\text{A}}$ to $6934\overset{\circ}{\text{A}}$ on cooling the ruby rod from room temperature to liquid N_2 temperature, it was suspected that excess heat from the flashlamp was

shifting the laser wavelength. This was checked by placing a constantan-copper thermocouple in the water coolant reservoir and an identical reference thermocouple in an ice-water bath. The voltage differences were measured using either a Fluke digital multimeter or Rubicon Instruments potentiometer. During the course of the five laser pulses that make up one O_2 data point, the water reservoir temperature was found to vary by as much as $0.5^\circ C$. The temperature from one O_2 data point to the next varied by as much as 1 to $2^\circ C$. In the neighborhood of $20^\circ C$, the laser wavelength as a function of temperature is given by;

$$\lambda(T) = 6943.25 + 0.068(T - 20) \quad (7)$$

for λ in \AA and T in $^\circ C$.³⁴ A change in temperature from 20 to $22^\circ C$ therefore corresponds to a wavelength shift of 0.136\AA or approximately twice the laser spectral bandwidth. To determine the effect of such a shift on O_2 formation, NO_2 of normal isotopic composition was photolyzed at laser temperatures $21.2 (\pm 0.5)^\circ C$ and at $25.3 (\pm 0.5)^\circ C$. The ratio of O_2 formed at these respective temperatures was found to be about 3.5 to 1.0. That such a change in the O_2 production occurs is evidence of fine structure in the NO_2 absorption spectrum in the neighborhood of 6943\AA .

2.3.3 Multiphoton Fluorescence Studies

The experimental procedure for the multiphoton emission studies was similar to that of the normal fluorescence studies. The photomultiplier output was displayed on a time-swept oscilloscope and the resulting trace photographed. The laser intensity was varied using the apparatus mentioned previously in section 2.3.2. From these experiments the fluorescent intensity dependence on laser intensity could be deduced.

Also measured was the observed decay time for the emission as a function of NO_2 pressure as well as the peak intensity as a function of NO_2 pressure.

The gas pressures used in these studies were considerably higher than in the normal fluorescence studies and a Decker Corporation differential pressure sensor with a less sensitive detector was used to measure the pressures.

The RCA 8575 PMT was used at 2300 V, and the Tektronix 7904 oscilloscope was used as mentioned earlier, making use of a trigger pulse from the Pöckels cell unit to initiate the oscilloscope sweep.

RESULTS

3.1 Fluorescence and Quenching of NO₂

In all cases, the signal from the photomultiplier tube was applied to the vertical axis of the oscilloscope and the time base swept at the desired speed. The resulting trace was photographed on Polaroid Type 47 black and white film using the Tektronix C-51 camera unit. The intensity versus time traces could be analyzed by selecting points and measuring the trace height, at a given time, using a Bausch and Lomb precision comparator, or alternatively, the traces could be projected, expanded, and traced on graph paper. Both methods were used, but the accuracy was limited in both cases by the finite width of the trace. Most of the data were taken directly off of the photographs using the precision comparator.

3.1.1 Self-Quenching of NO₂ at Low Pressures

An example of the low pressure NO₂^{*} fluorescence decay is shown in Figure 5. As can be seen from the log I versus time plot for this decay, shown in Figure 6, the decay is very close to a simple exponential decay and is assumed to be such.

For NO₂ at low pressures and for the quenching of NO₂ by foreign gases, a simple single excited state mechanism was used to analyze the data. This mechanism is given below:

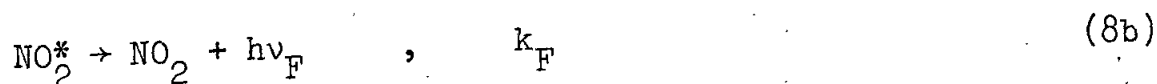
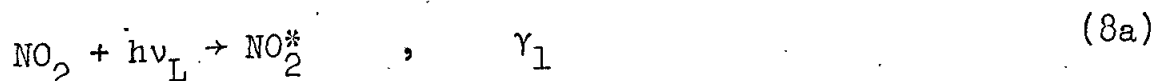


Figure 5 Typical Decay Curve

P = 25 mtorr

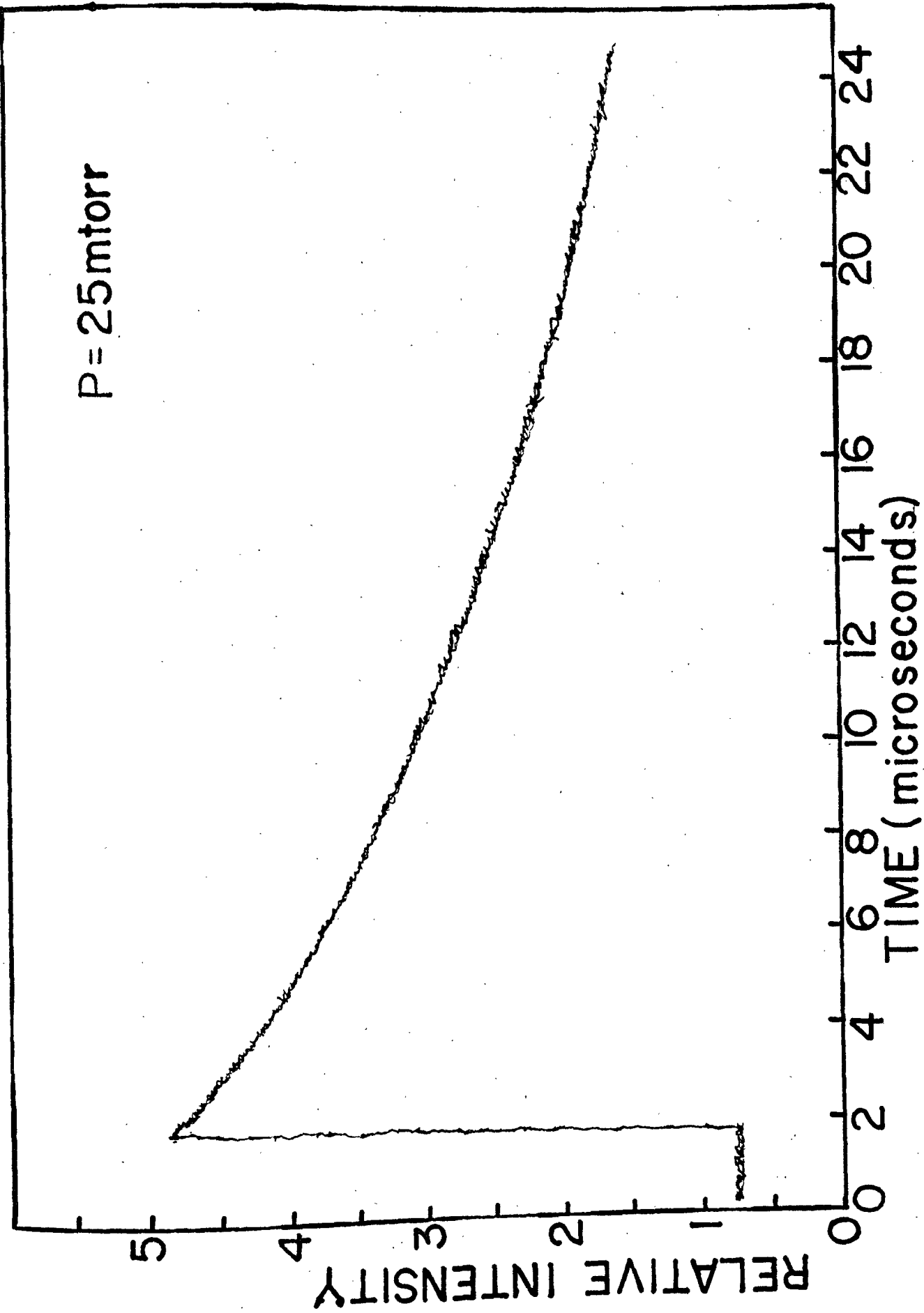
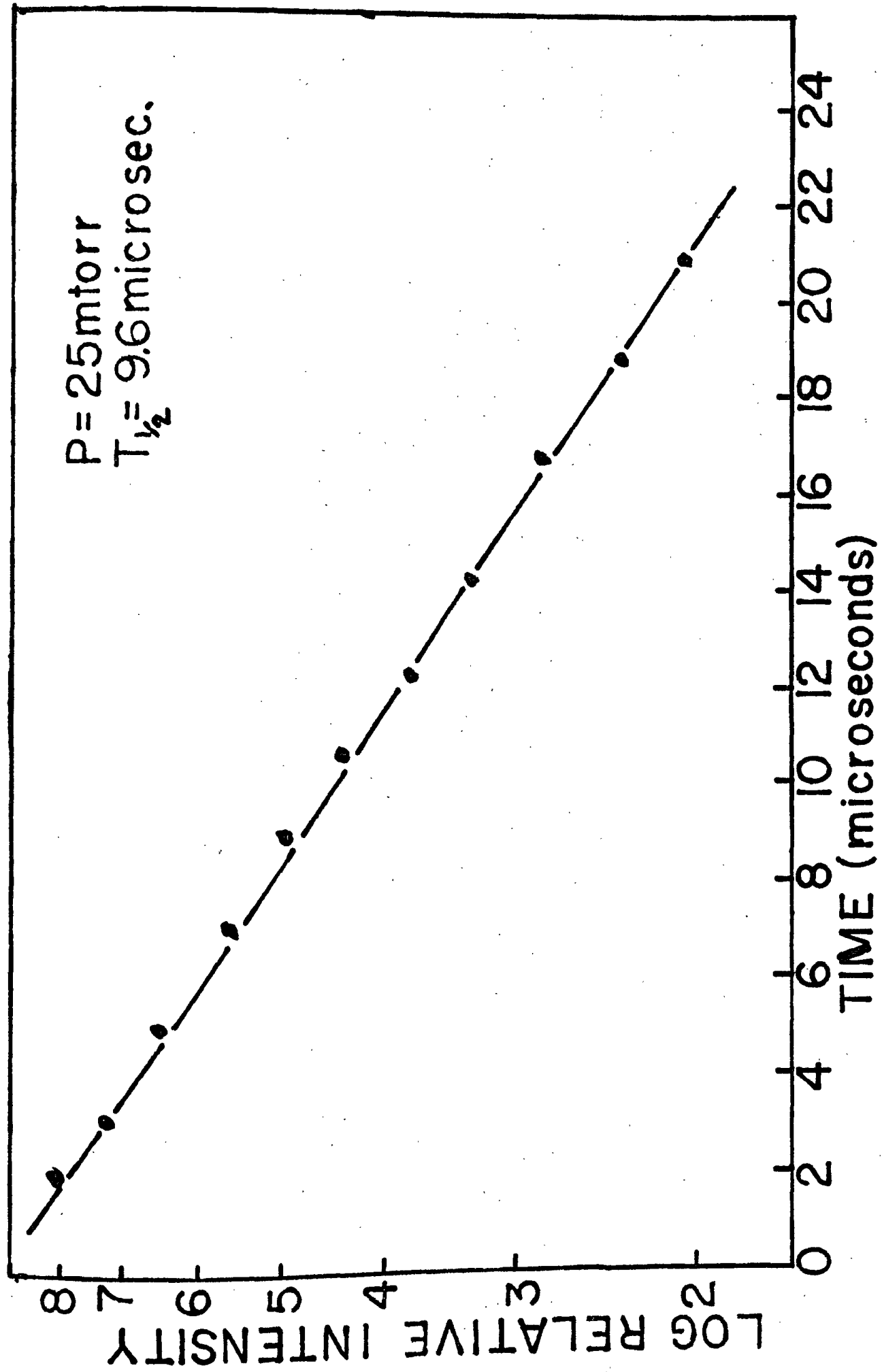


Figure 6 Typical Semilog Plot to Obtain Lifetime





Here γ_1 is the effective excitation rate, $k_F (= 1/\tau_0)$ is the fluorescence rate constant or the reciprocal of the collision-free radiative lifetime, τ_0 , and k_{Qi} is the quenching rate constant for the collision partner species, M_i .

Assuming the laser excitation to be rapid in comparison to subsequent relaxation processes allows one to express the rate equation of interest as being,

$$\frac{d(\text{NO}_2^*)}{dt} = -[k_F + \sum_{i=1}^N k_{Qi}(M_i)](\text{NO}_2^*) \quad (9)$$

which has the solution

$$(\text{NO}_2^*)_t = (\text{NO}_2^*)_0 \exp -[k_F + \sum_{i=1}^N k_{Qi}(M_i)]t. \quad (10)$$

Here $(\text{NO}_2^*)_0$ is the initial concentration of excited NO_2 formed by the essentially instantaneous laser excitation pulse. Since we have the relation,

$$I_F(t) \propto k_F(\text{NO}_2^*)_t \quad (11)$$

then a plot of $\ln I(t)$ versus time will be linear with a slope equal to $(-1/\tau_{\text{obs}})$, where

$$\frac{1}{\tau_{\text{obs}}} = k_F + \sum_{i=1}^N k_{Qi}(M_i) \quad (12)$$

For the low pressure self-quenching of NO_2^* the only (M_i) species of any consequence will be NO_2 since at most ~3% of the NO_2 molecules become excited. Equation (12) can be rewritten in this case to be,

$$\frac{1}{\tau_{\text{obs}}} = \frac{1}{\tau_0} + k_{Q_{\text{NO}_2}} (\text{NO}_2) \quad (13)$$

A plot of the experimentally measured value of $1/\tau_{\text{obs}}$ versus the NO_2 pressure should yield a straight line of intercept, $1/\tau_0$, and slope, $k_{Q_{\text{NO}_2}}$. This is a modification of the Stern-Volmer plot and the data are displayed in this manner as shown in Figure 7.

3.1.2 Quenching by Foreign Gases

To study the effect of foreign gas quenching on NO_2 fluorescence, a fixed amount of NO_2 was added to the sample cell and then the foreign gas was added, increasing the pressure at increments. The Stern-Volmer plot now can be written as follows:

$$\frac{1}{\tau_{\text{obs}}} = \left[\frac{1}{\tau_0} + k_{Q_{\text{NO}_2}} (\text{NO}_2) \right] + k_{Q_M} (M) \quad (14)$$

The term in brackets is a constant for any given experiment since (NO_2) is fixed and a $1/\tau_{\text{obs}}$ versus (M) plot should be a straight line of slope k_{Q_M} . The data for the foreign gases studied in this manner are shown in Figure 8 and 9. The values obtained for $1/\tau_0$, $k_{Q_{\text{NO}_2}}$, and the k_{Q_M} are summarized in Table 4.

3.1.3 Self-Quenching of NO_2 at High Pressures

The time-resolved emissions from NO_2^* at higher (> 50 mtorr) pressures were markedly non-exponential and Stern-Volmer models were inapplicable. In fact, an increase in emission intensity followed by a decay could be observed. Some selected traces are shown in Figure 10 for illustration. They show not only the appearance of one maximum in the intensity-time curve, but also the appearance of a second maximum

Figure 7 Stern-Volmer Plot for Pure NO_2

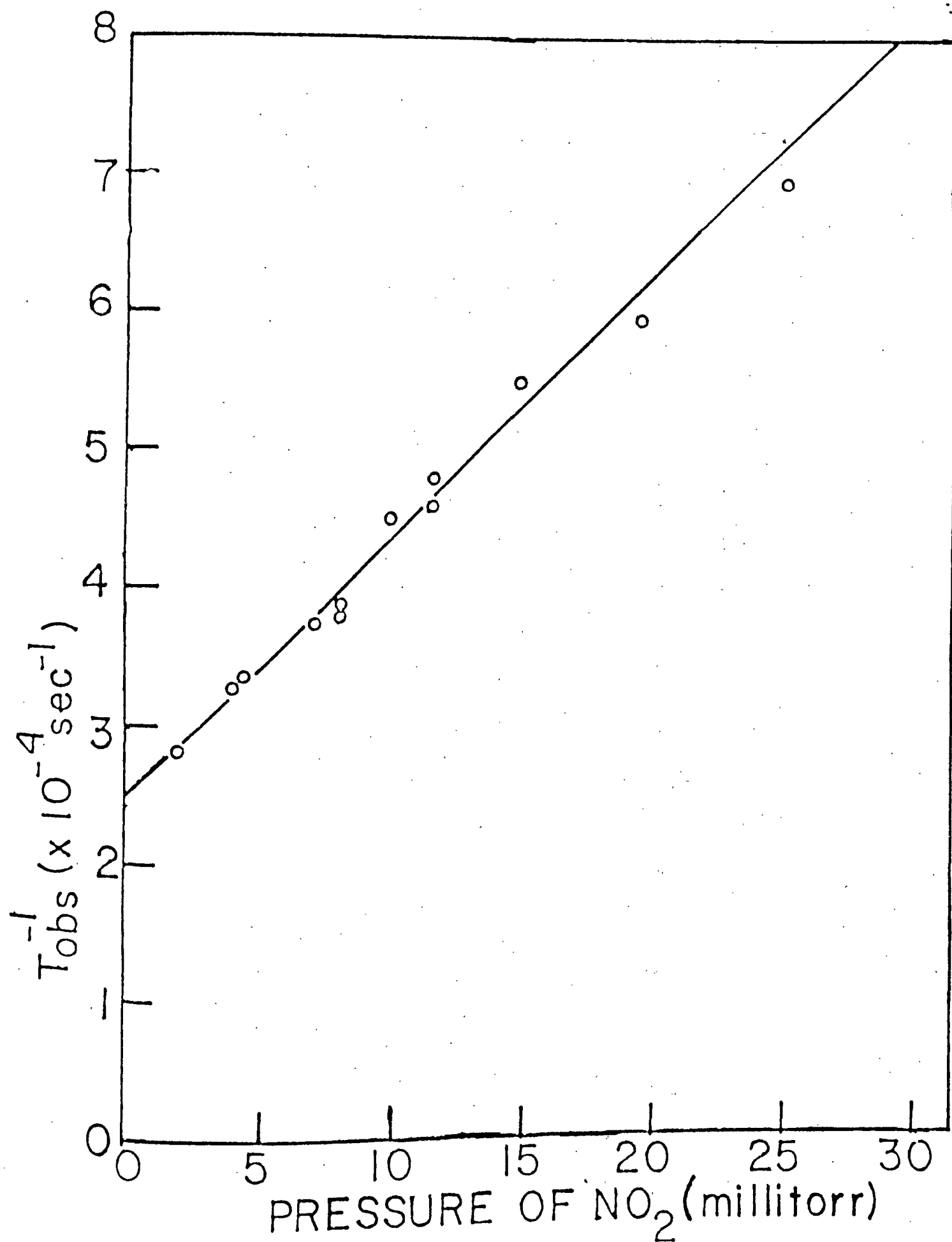


Figure 8 Stern-Volmer Plot for He, Ar, O₂, CO₂

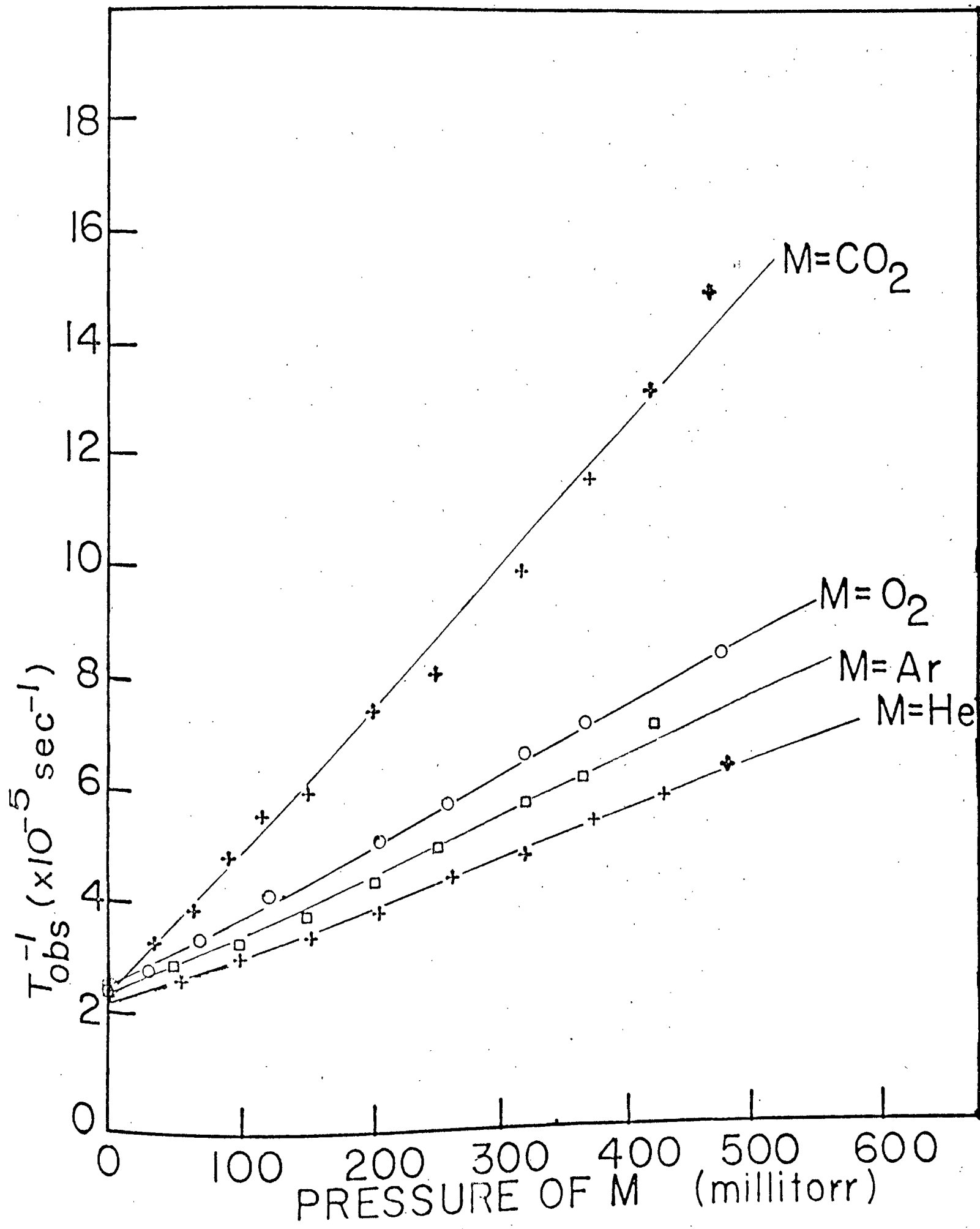


Figure 9 Stern-Volmer Plot for N_2 , CO, NO, N_2O

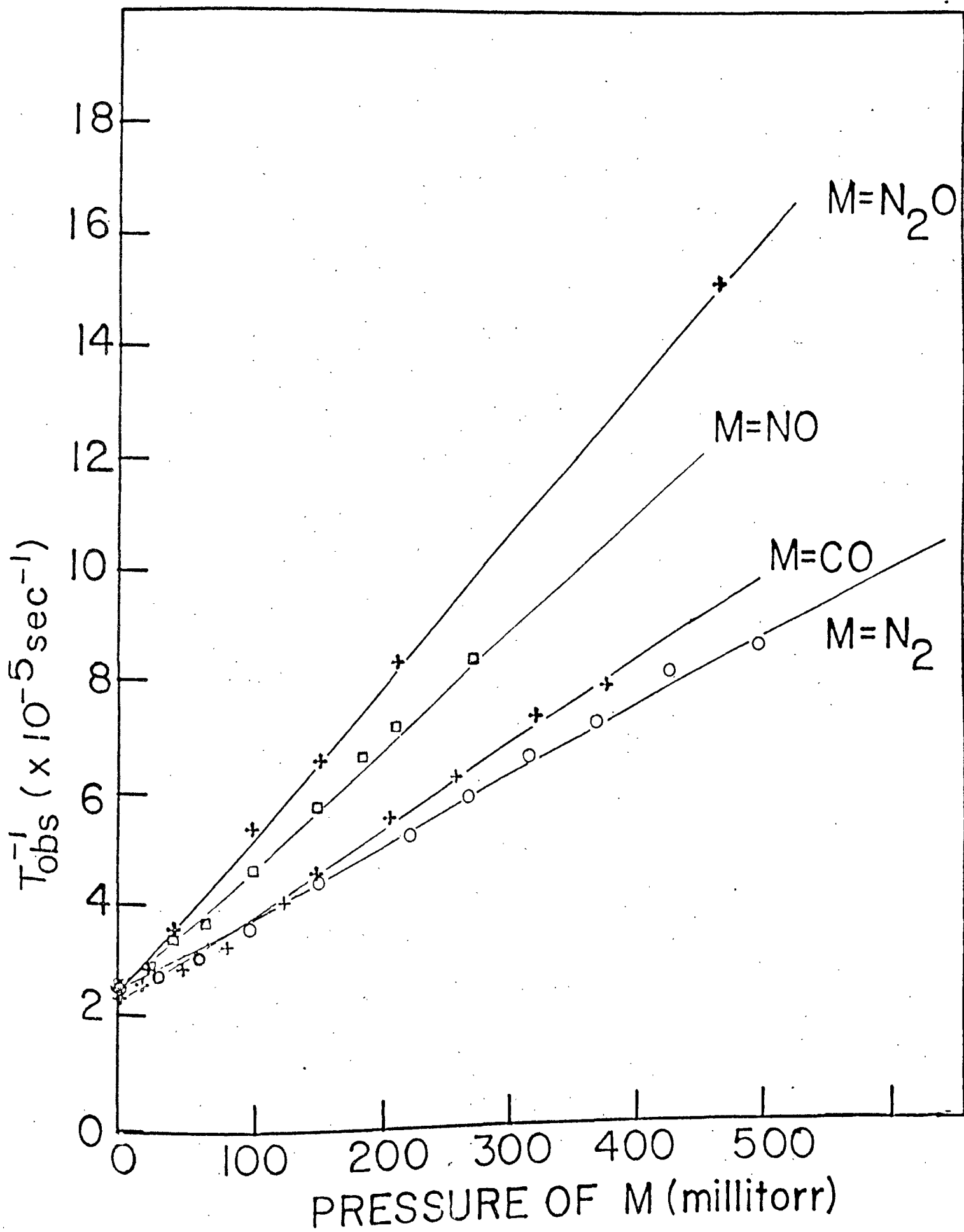


Table 4

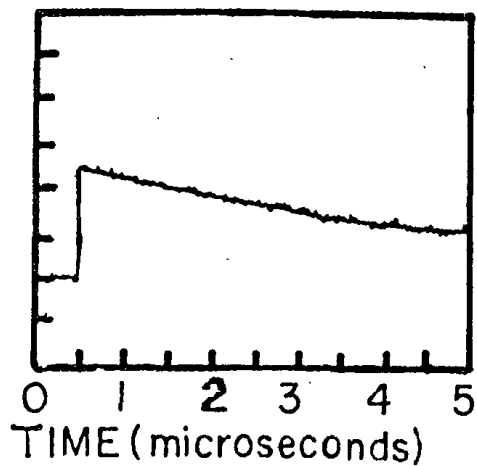
Quenching Rate Constants of NO* for a Series of Added Gases

<u>Gas</u>	<u>Mol. Wt.</u>	<u>Quenching Constant (cm³/part-sec)</u>
He	4	2.5×10^{-11}
Ar	40	3.2×10^{-11}
N ₂	28	3.9×10^{-11}
CO	28	4.8×10^{-11}
NO	30	6.7×10^{-11}
O ₂	32	3.6×10^{-11}
CO ₂	44	7.7×10^{-11}
N ₂ O	44	8.6×10^{-11}
NO ₂ ^(a)	46	5.7×10^{-11} ^(b)

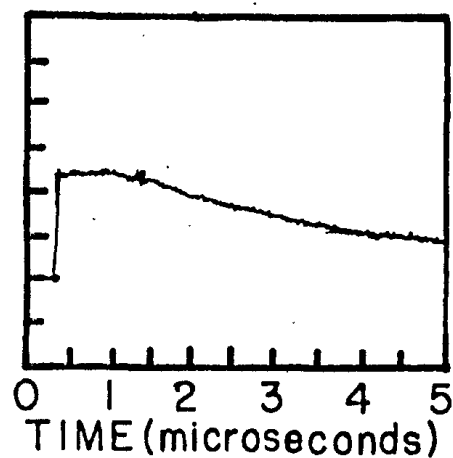
(a) The collision free radiative lifetime was determined to be 41 ± 4 microseconds.

(b) Due to rapid simultaneous vibrational deactivation this number is difficult to interpret in terms of solely electronic quenching.

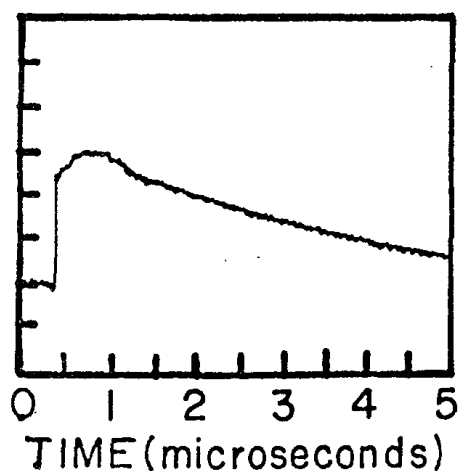
Figure 10 Sample Traces of Non-Exponential Decays



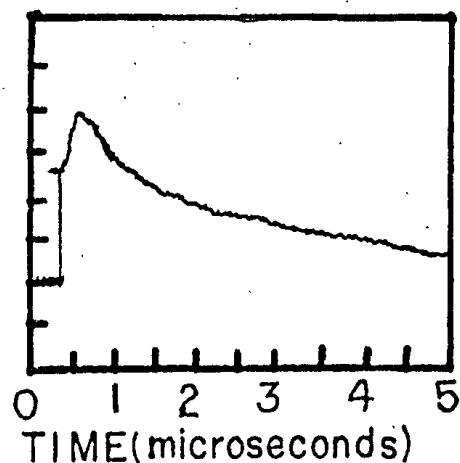
P = 25 mtorr



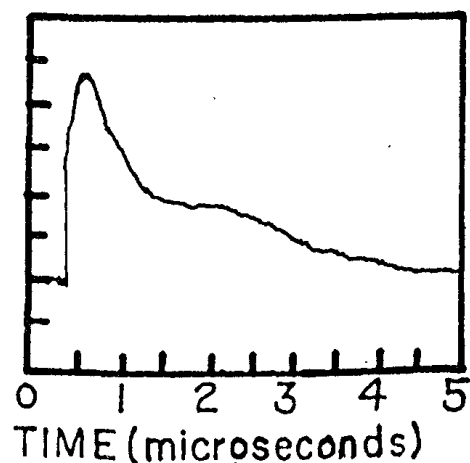
P = 41 mtorr



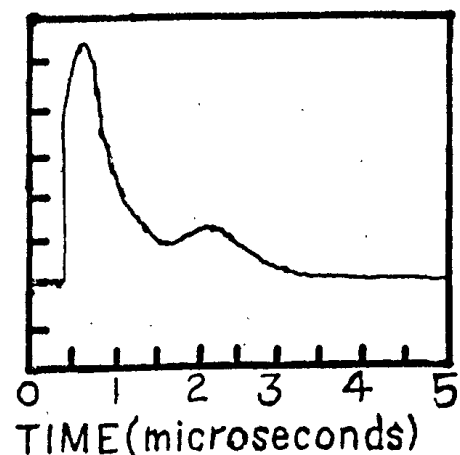
P = 50 mtorr



P = 61 mtorr



P = 110 mtorr



P = 220 mtorr

SAMPLE OSCILLOSCOPE TRACES

occurring at higher pressures and peaking at longer times than the first. A plot of the peak intensity of the first maximum versus pressure is given in Figure 11. This shows a linear dependence of peak height on NO_2 pressure at low NO_2 pressure, and a leveling off at higher NO_2 pressures. The break in behavior occurs at approximately the same pressure that the second maxima begins to occur.

The general appearance of these emission curves is reminiscent of a consecutive process wherein an intermediate is observed with greater sensitivity than other species. With the consecutive mechanism given below,



one can readily calculate the time for species B to reach maximum concentration as being,

$$\tau_{\max} = (\lambda_1 - \lambda_2)^{-1} \ln(\lambda_1/\lambda_2) \quad (16)$$

Assuming the pseudo-first order rate constants, λ , to be proportional to pressure, $\lambda = k(M)$, one can write the following;

$$\frac{1}{\tau_{\max}} = \left[\frac{(k_1 - k_2)}{\ln(k_1/k_2)} \right] (M) \quad (17)$$

The reciprocal of the measured time to maximum was plotted versus the NO_2 pressure and a linear relationship was found, as is shown in Figure 12. The rise-time to maximum and decay time after maximum can serve to give rough estimates of k_1 and k_2 independently. These estimates show k_1 to be about $6 \text{ to } 4 \times 10^{-10} \text{ cm}^3/\text{part-sec}$ and k_2 to be about $5 \text{ to } 3 \times 10^{-10} \text{ cm}^3/\text{part-sec}$. The interpretation of these results will be given later in the discussion.

Figure 11 First Maximum Peak Intensity Versus Pressure of NO₂

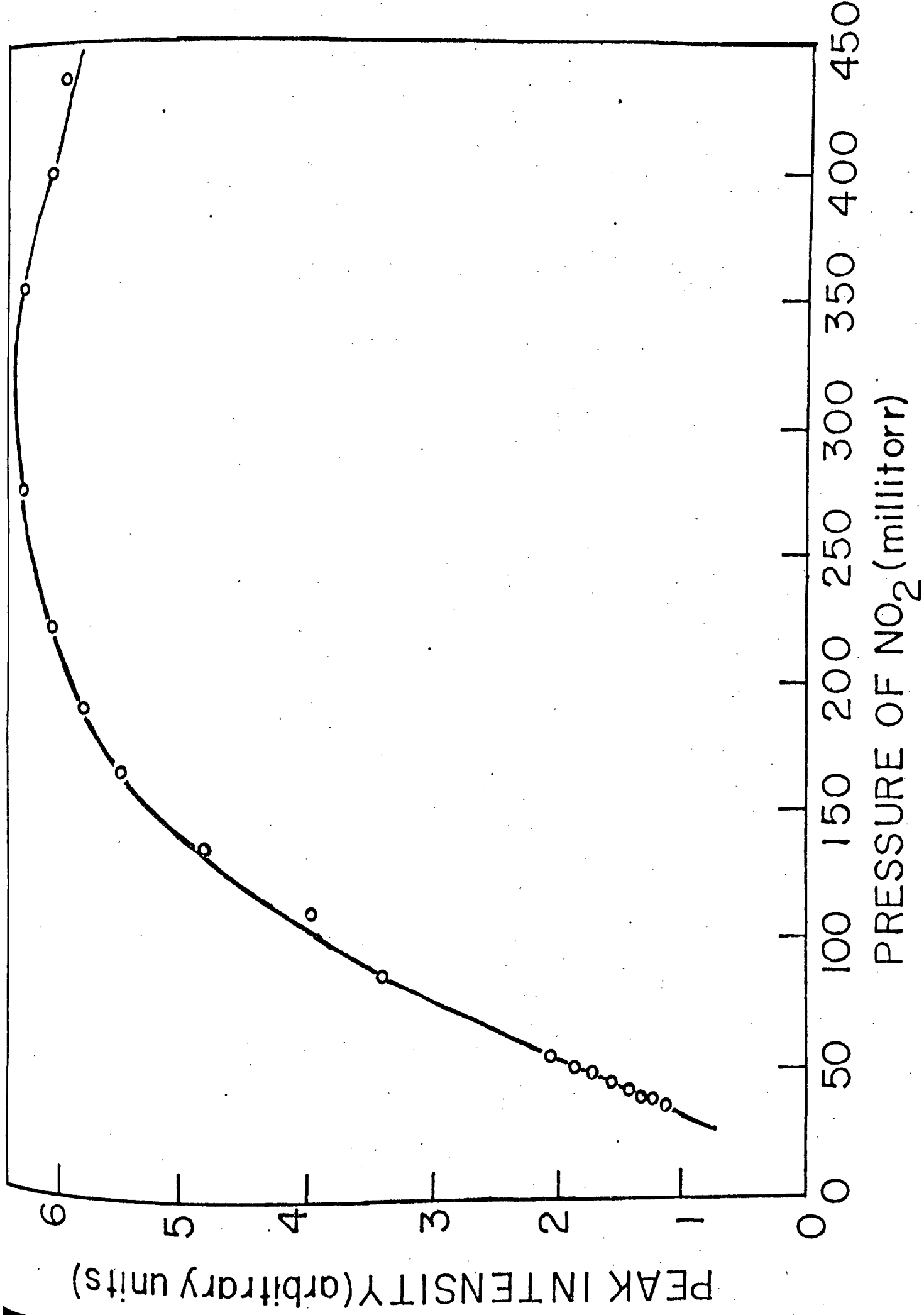
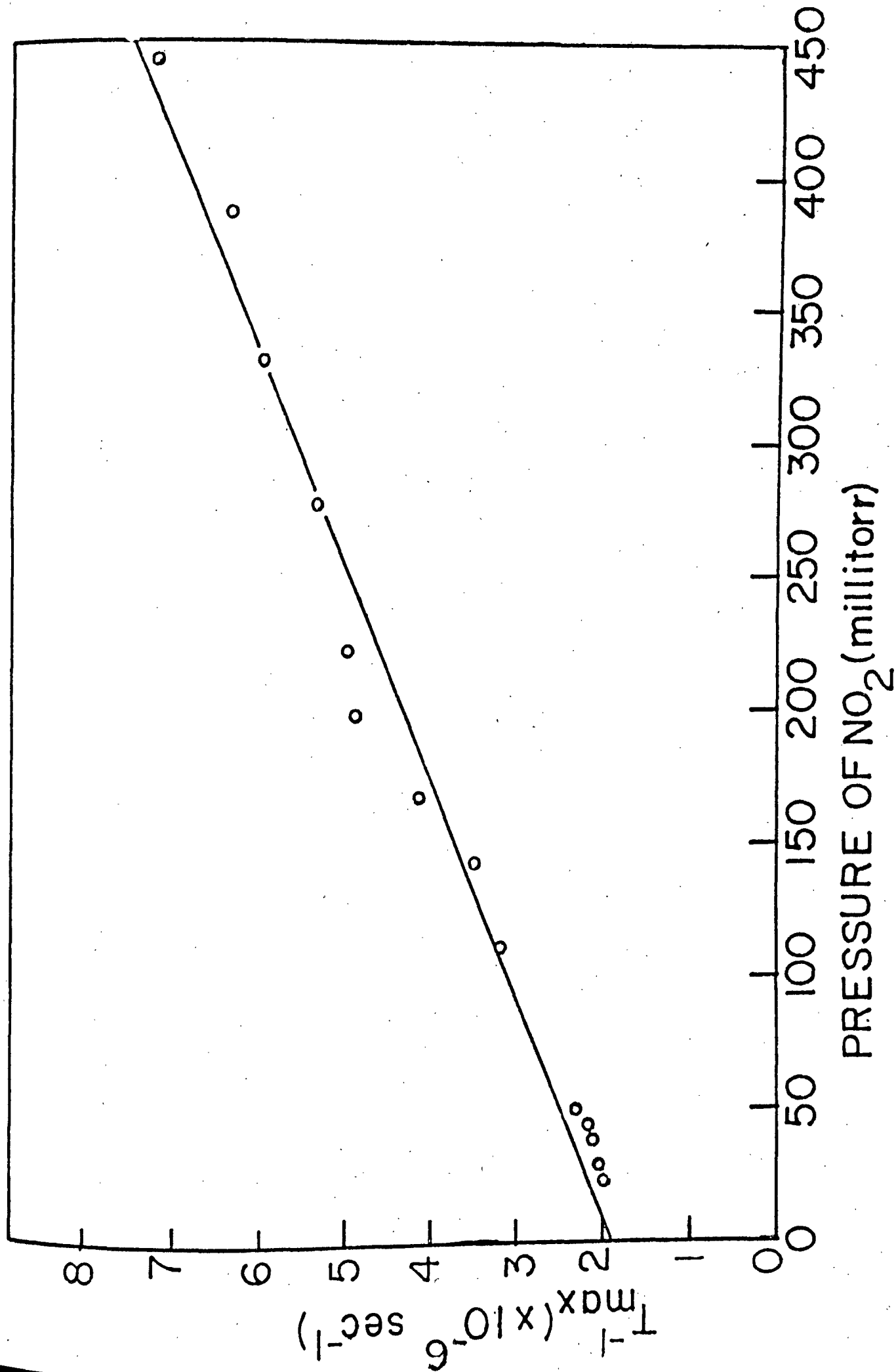


Figure 12 . Inverse Time to First Maximum Versus Pressure of NO₂



3.2 Two-Photon Induced Dissociation of NO₂

The amount of O₂ formed as a result of five laser pulses was measured as a function of NO₂ pressure. These data are presented in Figure 13. These experiments were essentially a repeat of earlier work by Gerstmayr, et al, but using the Pöckels cell Q-switch instead of the cryptocyanine dye cell Q-switch. The result of this is a broader spectral width, a longer pulse duration, but a much more reproducible pulse energy. The comparison of results is therefore of interest and will be discussed later.

The variation of O₂ production with laser intensity was also measured, using the apparatus mentioned earlier. The results of these measurements are given in Figure 14 in the form of a $\log O_2$ versus $\log I_L$ graph. If the dependence of O₂ on laser intensity can be expressed as follows;

$$(O_2) = kI_L^n \quad (18)$$

then a $\log(O_2)$ versus $\log I_L$ plot should give a straight line of slope = n. The least square value for the slope obtained from the data was 2.00 (± 0.053), indicating the occurrence of at least a two photon process.

The isotope effect experimental results are best presented as the ratio of the m/e = 34 peak resulting from $(O^{16}O^{18})^+$ and the m/e = 32 peak resulting from $(^{16}O_2)^+$. These ratios are shown in Table 5 for several laser experiments as well as for the sunlight photolysis experiment.

Figure 13 Formation of O_2 Versus Pressure of NO_2

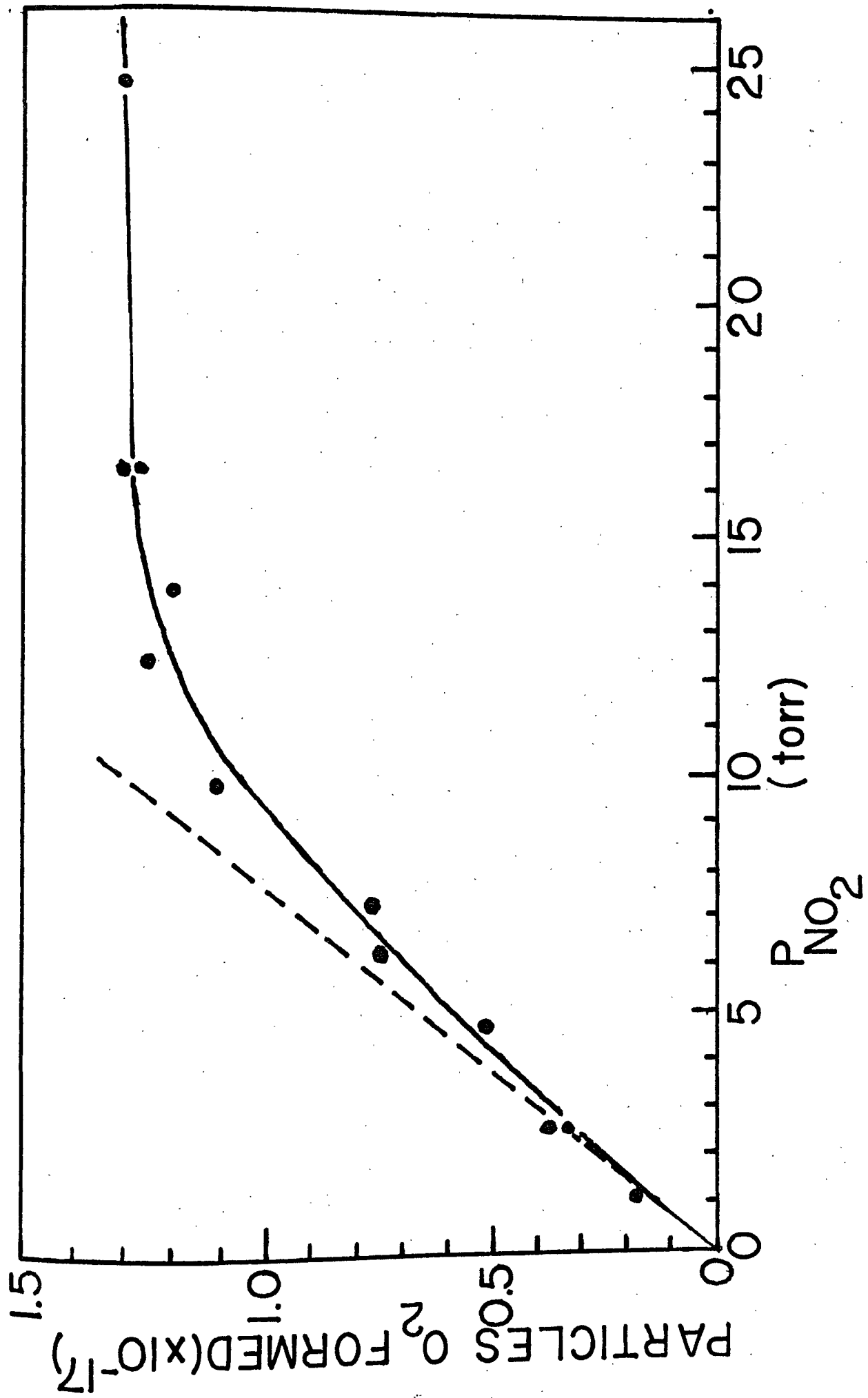


Figure 14 Log of O_2 Formed Versus Log of Relative Laser Intensity

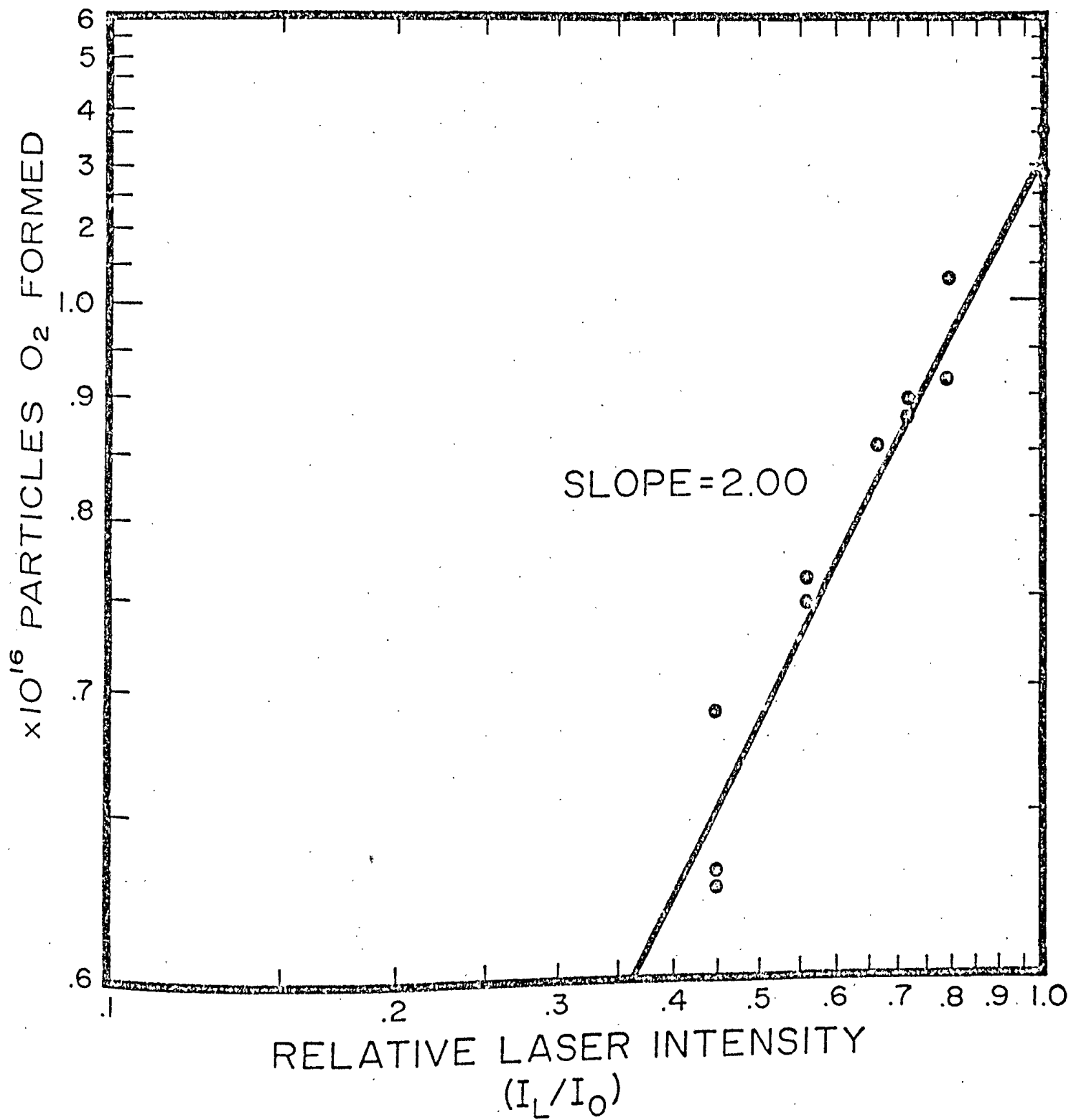


Table 5

Isotope Effect on O_2 Production

<u>Experiment</u>	<u>R ($m/e = 34/m/e = 32$)*</u>	<u>Comments</u>
1	0.546	Laser 5x
2	0.471	Laser 5x
3	1.10	Laser 5x
4	0.398	Sunlight (25 minutes)

* The calculated theoretical R value assuming a random, non-selective photolysis for the specific mixture composition used is $R = 0.400$.

3.3 Multiphoton Induced Fluorescence of NO₂

Attempts at observing a multiphoton induced emission in NO₂ were successful, but the results were not easy to interpret nor were they like anything that might be expected from comparison with other studies.

The variation of emission intensity with NO₂ pressure is shown in Figure 15. The low pressure intensity dependence could be first or second with respect to pressure or some intermediate value, the data are not accurate enough to decide. The dropping off of intensity at higher pressures is most likely due to self-absorption by the NO₂ since it absorbs strongly in the 4000 to 4400 Å region, the absorption coefficient being about a factor of 100 times greater than in the 6943 Å region.

The Stern-Volmer plot of observed lifetime versus pressure was linear to about 30 torr, above which the lifetime was comparable to the laser pulse duration and could not be separated out readily. The emission was observable only at higher pressures so a low pressure extrapolation to obtain a value for τ_0 in this region was very difficult with the present arrangement. However, from the Stern-Volmer plot of the emission, as shown in Figure 16, a value for the effective quenching constant of $k_Q = 2.5 \times 10^{-11} \text{ cm}^3/\text{part-sec}$ could be obtained.

The variation of fluorescence intensity with laser intensity was measured using the apparatus mentioned in section 2.3.2 at a series of different pressures and the results are presented in Figure 17 in the form of a $\log I_F$ versus $\log I_L$ graph. This shows the interesting result that the order with respect to laser intensity varies from 3.0 at low pressure to a limiting value of 2.0 at high pressure as shown in Figure 18.

Figure 15 Blue Fluorescence Intensity Versus Pressure of NO₂

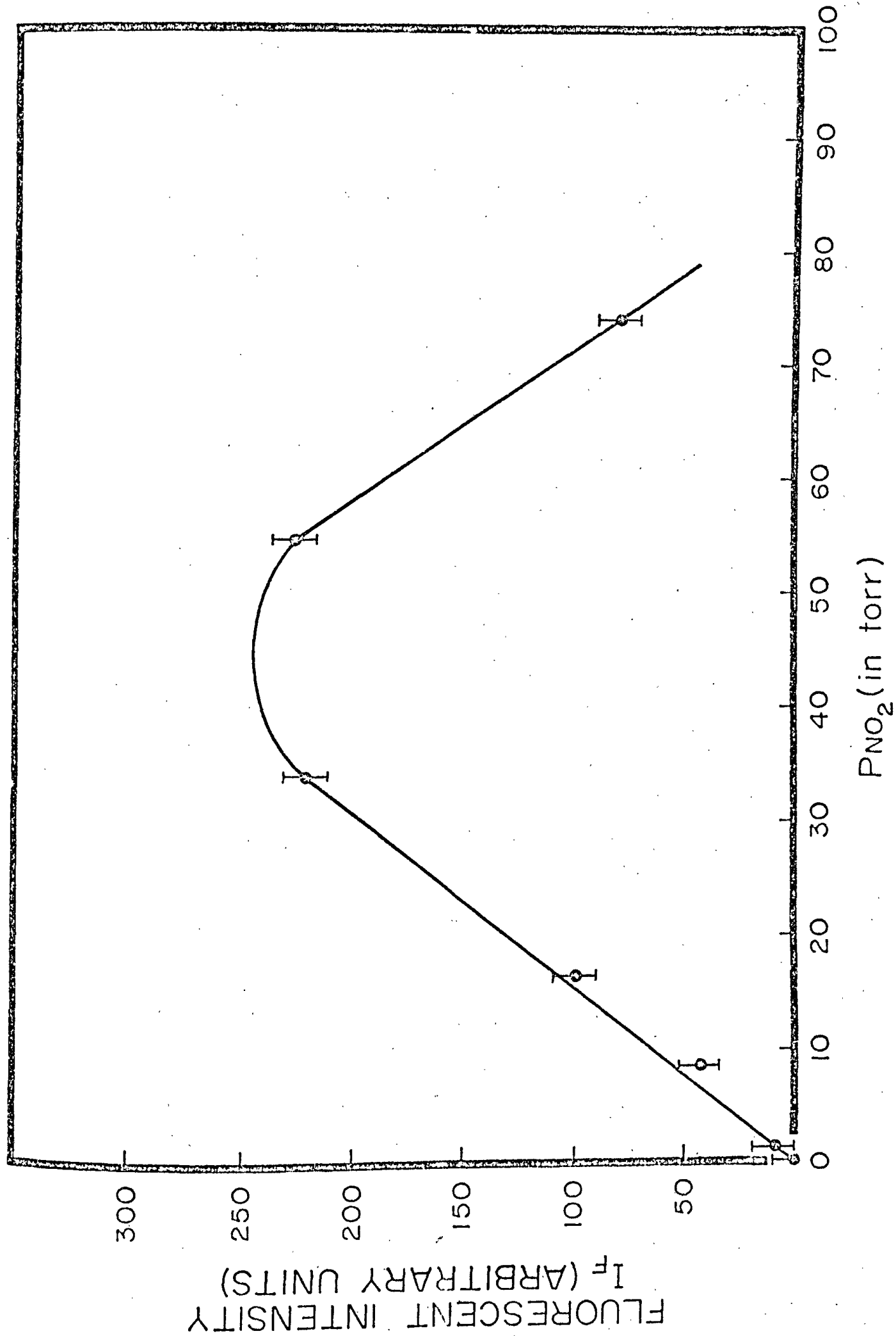


Figure 16 Stern-Volmer Plot for the Blue Emission

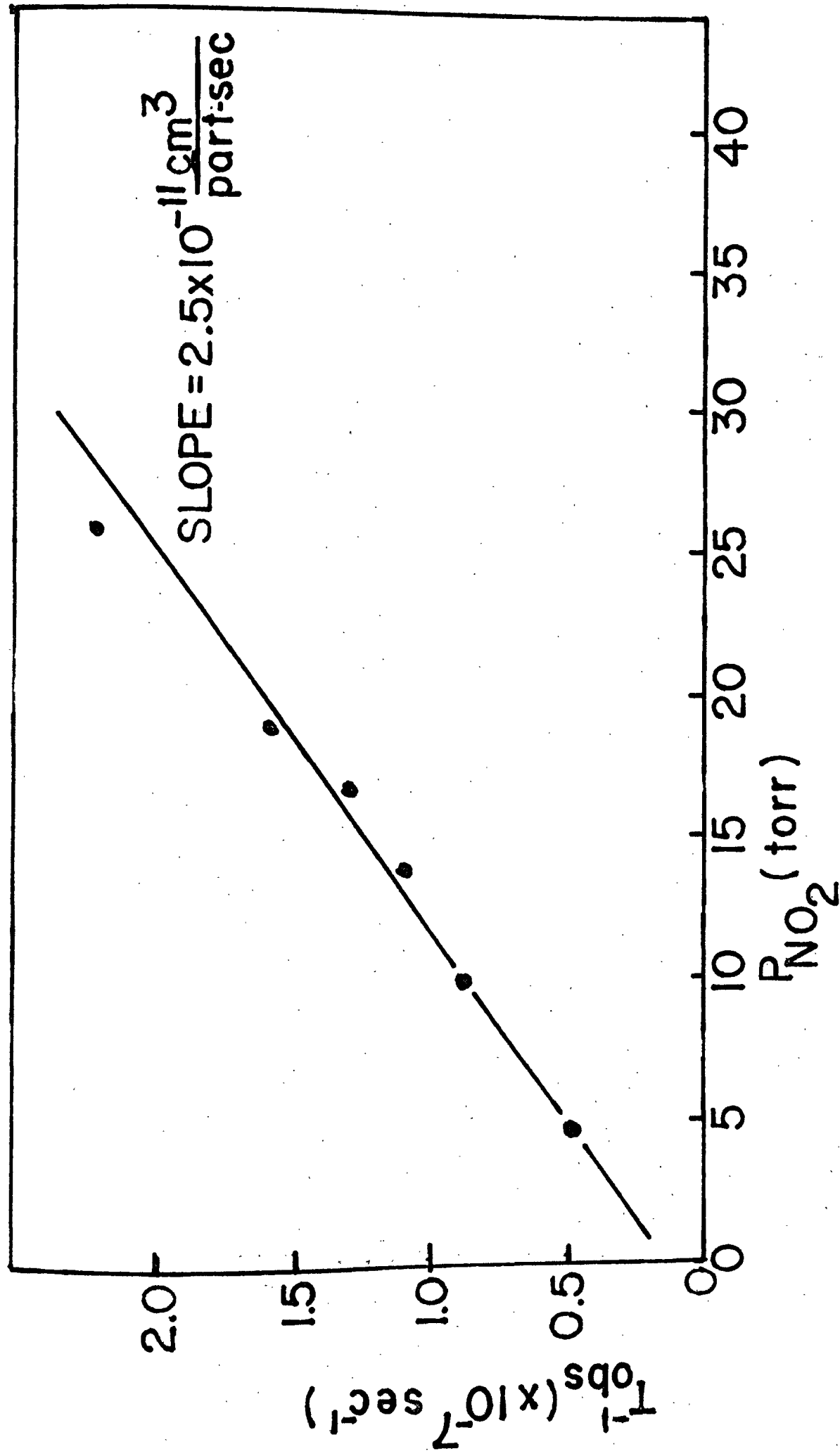


Figure 17 Log of the Blue Fluorescence Intensity Versus Log of the
Relative Laser Intensity for Various Pressures of NO₂

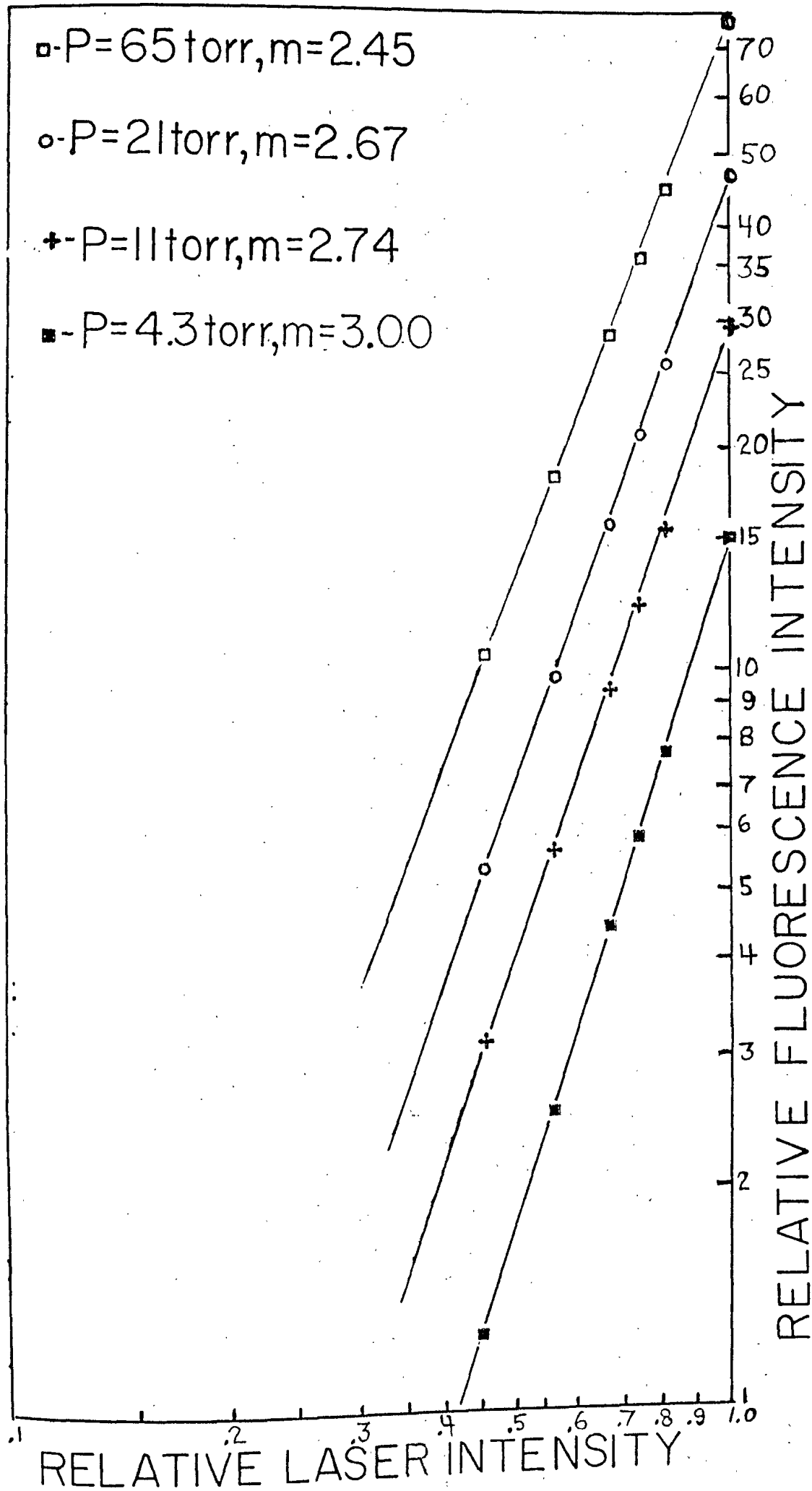
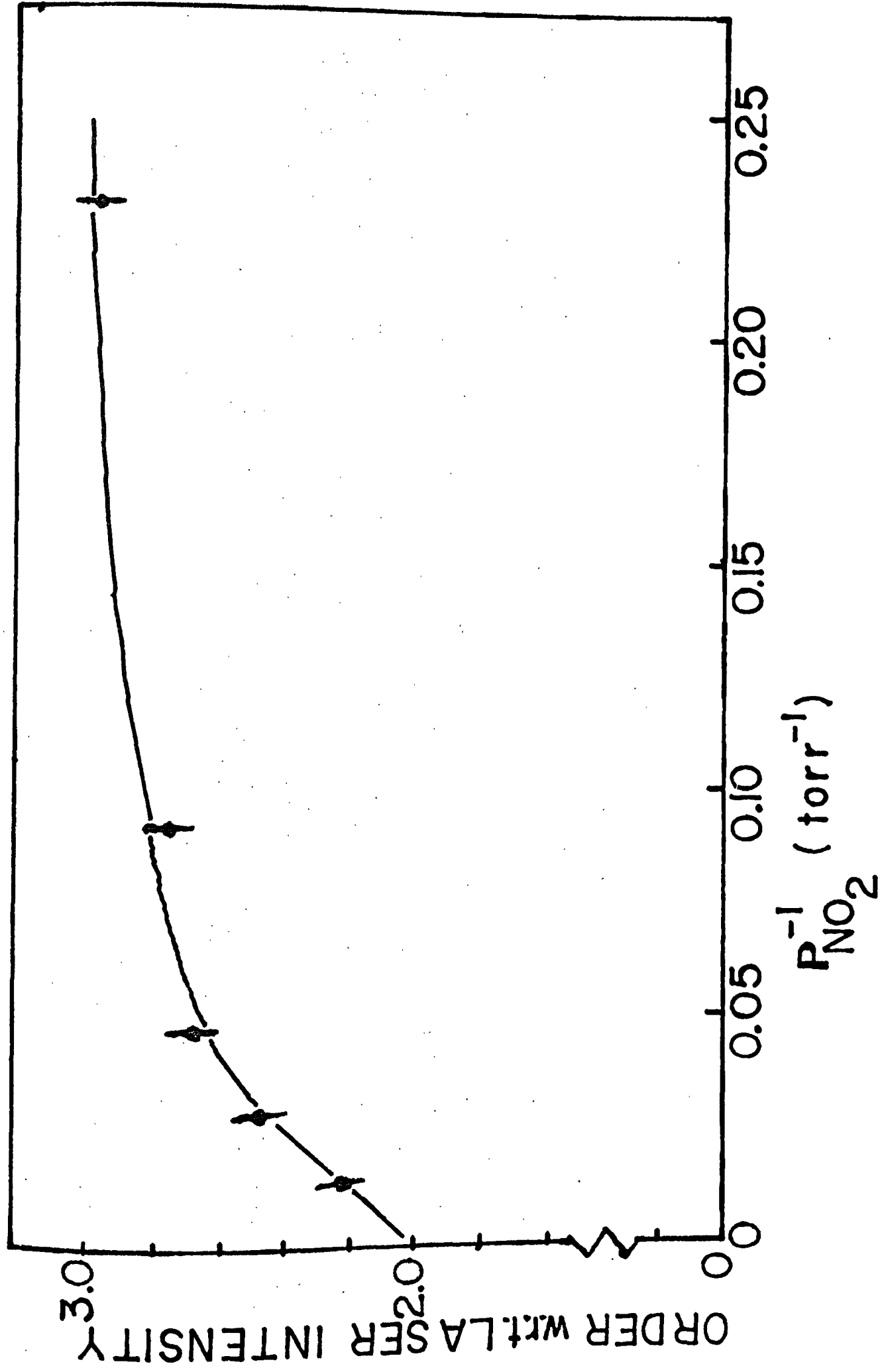


Figure 18 Order of the Blue Emission Intensity with Respect to Laser
Intensity Versus the Inverse of the NO_2 Pressure



If we consider the fluorescent intensity to be due to the sum of a three photon and a two photon process as follows;

$$I_F = C_1 I_L^2 + C_2 I_L^3 \quad (19)$$

then a plot of I_F/I_L^2 versus I_L will give a slope equal to C_2 and intercept C_1 . The ratio (C_2/C_1) will be a measure of the relative importance of the three photon to two photon process at any given pressure. These data are presented in Table 6 and show that the ratio (C_2/C_1) is inversely proportional to pressure, or that the two photon process depends on pressure to one order higher than the three photon process.

Table 6

<u>Ratio (C_2/C_1)</u>	<u>P (torr)</u>
6.19	4.3
3.12	10.8
1.07	20.6
0.51	65.1

$$\frac{C_2}{C_1} = \frac{25.2}{P \text{ (in torr)}}$$

DISCUSSION

4.1 Fluorescence of NO₂

Recent spectroscopic studies on the fluorescence and absorption spectra of NO₂ excited by several cw laser lines have placed the (0,0,0) level of the electronically excited 2B_1 state at 14,743 cm⁻¹ and the (0,0,0) level of the 2B_2 state at 11,956 cm⁻¹ for $^{14,16}_0N_2O_2$.^{11,12} The ruby laser line at 6943 Å corresponds to 14,403 cm⁻¹ and can excite the 2B_1 state only via a hot band transition. The (0,0,0) level of the 2B_1 state was obtained by extrapolation from shorter wavelengths since the 2B_1 state is apparently not responsible for any but a small percentage of absorption in the 6,000 to 11,500 Å region.¹¹ Very weak absorption is observed at wavelengths longer than 8365 Å (11,956 cm⁻¹) and is attributed to hot band transitions to the 2B_2 state.¹² On the basis of these other works it will be assumed here that the 2B_2 state is selectively populated by absorption of the ruby laser line. This differentiates results obtained with a ruby laser from all other previously used excitation sources in that other sources will excite both the 2B_1 and 2B_2 states simultaneously to some degree.

Observations on the fluorescence spectra and lifetime of NO₂ as excited by a variety of pulsed and continuous wave lasers have led to the following conclusions:

- (1) The fluorescence spectra of the 2B_1 state tend to be continuous, at least under the spectral resolutions used.^{11,35}
- (2) The fluorescence from the 2B_2 state tends to show a higher degree of banded structure than the 2B_1 state.³⁶

(3) The continuum emission (${}^2B_1 \rightarrow {}^2A_1$) tends to be of longer lifetime (up to 110 microseconds) than that of the more discrete emission (${}^2B_2 \rightarrow {}^2A_1$), which has shown lifetimes in the 0.5 to 3.7 microsecond range as well as 30 to 60 microsecond lifetimes.^{37,38}

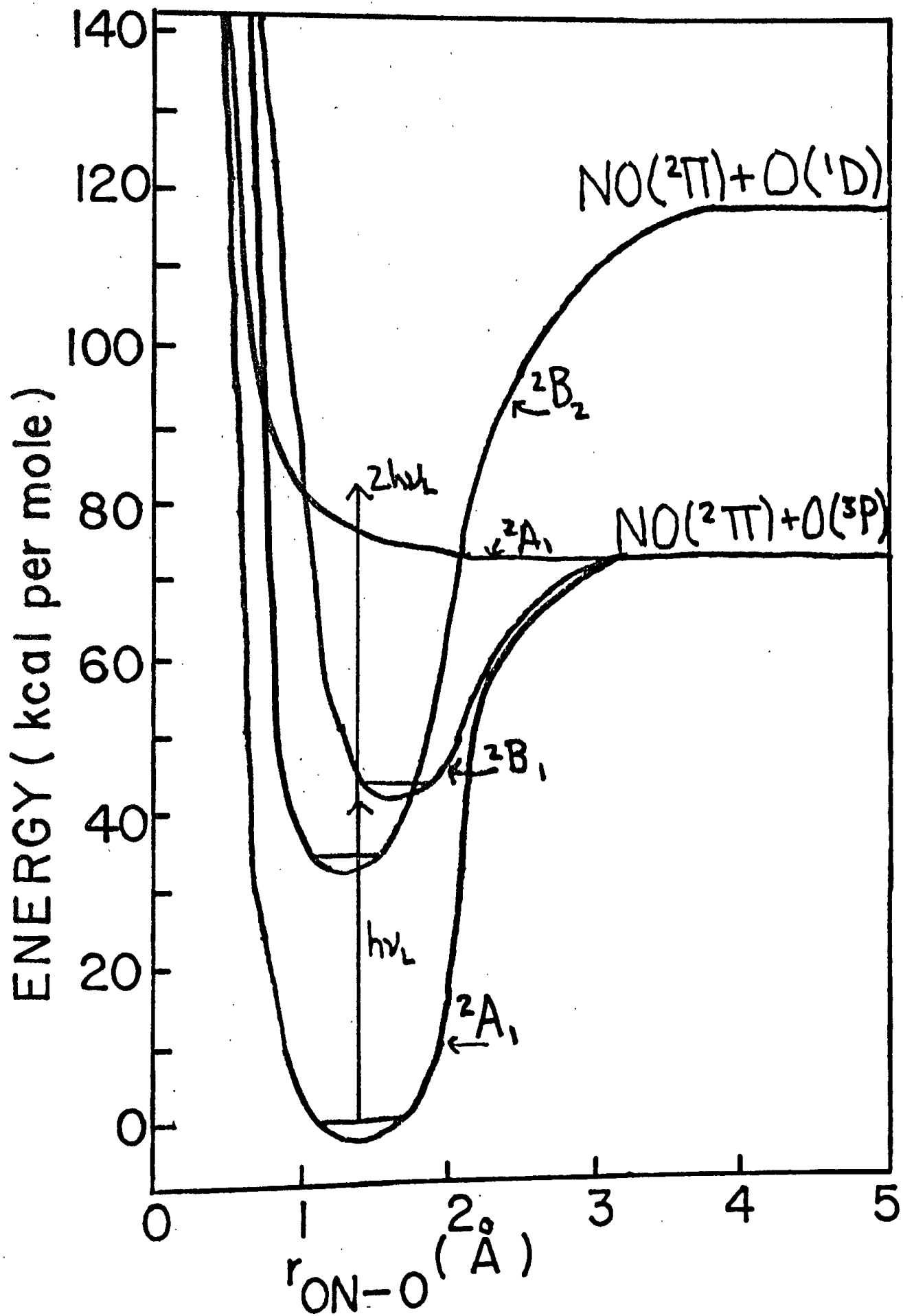
(4) The continuum (${}^2B_1 \rightarrow {}^2A_1$) emission is not quenched by the presence of a magnetic field, whereas the more discrete emission (${}^2B_2 \rightarrow {}^2A_1$) is quenched by a magnetic field.^{38,39} This implies that the 2B_1 state is already highly mixed with the 2A_1 state, but that the magnetic field perturbation induces a greater amount of ${}^2B_2 - {}^2A_1$ interaction.

(5) At higher NO_2 pressures, the presence of collision induced lines has not been observed.^{40,41} That fairly rapid vibrational deactivation occurs in NO_2^* has been previously established. The collision, therefore, must distribute the deactivated molecule over many rotational levels giving rise to no sharp new lines in the fluorescence spectrum, but only a rise in the continuum level (which may not be readily detected). Figure 19 shows an approximate potential energy diagram for NO_2 looking along the ON-O bond coordinate. Naturally a polyatomic is much more complex than this diagram implies, but it may aid in a visualization of processes that will be discussed.

4.1.1 Radiative Lifetime

The radiative lifetime obtained experimentally in this work for excitation at 6943\AA^0 was $41 (\pm 4)$ microseconds, which is substantially longer than the 0.25 microsecond lifetime estimated from the integrated absorption coefficient calculations made by Neuberger and Duncan although they obtained an experimental τ_0 of 44 μsec .⁴ However, Sakurai and

Figure 19 Approximate Potential Energy Diagram for the ON-O Bond

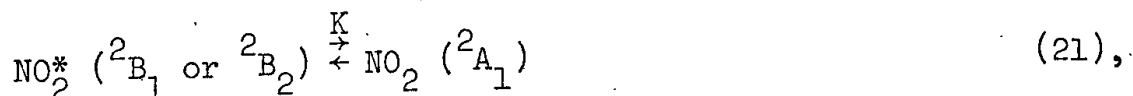


Broida's measurements on some selected line absorption coefficients lead them to believe that the earlier measurements may have been performed incorrectly, and that a lifetime on the order of several tens of microseconds could be expected.⁴¹

Douglas, in a theoretical discussion, attempted to explain the lifetime lengthening effect as being due to isoenergetic transitions between the vibronic levels of the upper electronic state and high vibrational levels of the lower electronic state.⁴² Since to a first-order approximation the Fermi Golden Rule gives the transition probability as being,⁴³

$$\omega_{i \rightarrow f} = \frac{4\pi^2}{h} |\langle f | H' | i \rangle|^2 \rho_f(E) \quad (20),$$

where H' is the perturbation and $\rho_f(E)$ is the energy density of final states, the equilibrium constant for the intramolecular transition,



will be the ratio of the density of energy levels of the 2A_1 state to that of the excited state. In general, the ground state will have a higher energy level density at a given energy and the NO_2^* will therefore spend more of its time in upper vibrational levels of the ground state due to the higher density of states where it cannot readily radiate. As a result the radiative lifetime is increased by the factor, $(K + 1)$.⁴⁴

The perturbing Hamiltonian, H' , that induces internal conversion and intersystem crossing processes is usually taken to be the nuclear kinetic energy operator and any spin-orbital interaction operators. It is the separation of nuclear and electronic kinetic

energies that forms the basis of the Born-Oppenheimer approximation, and it is the breakdown of this assumption that allows the zero-order Born-Oppenheimer states to undergo these transitions.⁴⁵

The degenerate ${}^2\Pi_u$ state of the linear NO_2 molecule correlates to the C_{2v} symmetry species, 2B_1 and 2A_1 , in the bent molecule. The Renner-Teller effect has been invoked to explain the apparently effective mixing of the B_1 and A_1 states with resulting lengthening of the apparent radiative lifetime in both NO_2 and SO_2 .⁴⁶ The experimental data of Schwartz and Senum of NO_2 fluorescence excited by a He-Cd laser at 4420\AA gives a lifetime of 36 microseconds for a 2B_1 vibronic level and supports this mechanism.⁴⁷

The Renner-Teller effect cannot be used as an explanation for the lifetime lengthening of the 2B_2 state, but the Herzberg-Teller effect wherein the upper vibronic levels of the ground state interact with and thereby perturb the vibronic levels of the upper electronic state was suggested as an explanation for the irregularity of vibrational structure in the longer wavelength absorptions to the 2B_2 state.¹² Such perturbations can act not only to shift energy levels but also to lengthen the lifetime according to the mechanism of Douglas. However, the mixing of 2B_2 and 2A_1 states would not be expected to be as strong or as regular as between the 2B_1 and 2A_1 states.

The radiative lifetime of a molecule can be expressed as follows:

$$\frac{1}{\tau_0} = \frac{64\pi^4}{3hc^3} |\bar{R}_e|^2 \sum_{v''} v_{v',v''}^3 q_{v',v''} \quad (22),$$

where \bar{R}_e is the electronic transition moment when the molecule is in its equilibrium configuration, $\nu_{v',v''}$ is the frequency of the transition $v' \rightarrow v''$, $q_{v',v''}$ is the Franck-Condon factor (square of the vibrational wavefunction overlap integral) for the transition $v' \rightarrow v''$, v' is the vibronic state that is radiating, and the v'' are the vibronic states to which it may radiate.⁴⁸

The fact that the absorption for NO_2 drops off in the red spectral region is indicative of the lower Franck-Condon factors as compared to the visible absorption towards the blue. The radiative lifetime for levels excited near the bottom of the ${}^2\text{B}_2$ state will be lower due to the smaller Franck-Condon factors and due to the fact that the transition probability is proportional to the third power of the frequency. If the Franck-Condon factor for a transition to a higher vibrational level in the ground state is larger than that for a transition to a lower level, the ν^3 factor may nevertheless force the molecule to radiate from the levels with small Franck-Condon factors. All of the above qualitative arguments are to illustrate that the lifetime of the NO_2^* formed by the ruby laser may be longer than that obtained from the integrated absorption measurements without invoking a mixing of states argument. However, if, for example, we take a mean frequency of 5000\AA for the fluorescence excited by a 4358\AA line and a mean frequency of $15,000\text{\AA}$ for the fluorescence excited by a 6943\AA line then the ν^3 factor introduces a factor of 27 into the relative transition probabilities. This alone is not enough to explain the factor of ~ 160 difference in comparing the 41 microsecond with the 0.26 microsecond lifetime.

A combination of all these factors, the mixing of states, the v^3 effect, and inaccuracies in the integrated absorption coefficient measurements, may all contribute to explaining the discrepancy. The important result is that the $\text{NO}_2^* (^2\text{B}_2)$ which should not mix strongly with the $^2\text{A}_1$ ground state shows a radiative lifetime in the order of 40 microseconds using excitation at 6943\AA and that this lifetime differs by a factor of two or so from most other measurements of the excited state lifetime for any wavelength excitation.

4.1.2 Quenching of NO_2 Fluorescence

The electronic quenching rate constants for a series of added gases were determined experimentally and tabulated above. Many of the gases studied here were also studied by Myers, Silver, and Kaufman in a steady-state irradiation of NO_2 at 4358\AA , and a comparison of results may be appropriate.⁵ No other study of foreign gas quenching of NO_2^* has been performed.

The early theory of Rössler stated that the probability of quenching per collision was proportional to α , the polarizability of the quencher and the collisional duration, which is proportional to $\mu^{1/2}$, the square root of the reduced mass of the collision pair.⁴⁹

More recently Steinfeld and Selwyn have examined the quenching phenomena as being radiationless transitions induced by van der Waals interactions between the collision pair.⁵⁰ More specifically, a parametric dependence is found for the quenching cross-section:

$$\sigma_Q \propto \frac{\mu^{1/2} I \alpha}{R_0^3} \quad (23),$$

where σ_Q is the quenching cross-section, μ is the reduced mass, I is the ionization potential of the quencher, α is the polarizability of the quencher, and R_0 is the gas-kinetic distance of closest approach.⁵⁰

The quenching constants and cross sections, obtained in this work given in Table 7 along with the ratio of these cross-sections to those of Myers, Silver, and Kaufman.⁵ Some of these cross-sections for the data obtained here and the data obtained by Myers, Silver, and Kaufman are plotted in Figure 20 in the form of $\log \sigma_Q$ versus $\log \left[\frac{\mu^{1/2} I \alpha}{R_c^3} \right]$. Although log-log plots tend to make almost anything look like a reasonable correlation, a similar plot of the data using a $\log \sigma_Q$ versus $\log(\alpha \mu^{1/2})$ plot which has been used as a correlation for I_2^* quenching gives terrible results in comparison. Steinfeld's theory gives, at least in the case of NO_2^* , a reasonable correlative agreement with experiment.

The study of NO_2^* quenching by Sakurai and Broida indicated that the cross-sections for self-quenching of narrow-band discrete emission features were about 15 to 20 \AA^2 , whereas the self-quenching of apparently continuous emission was about 0.9 \AA^2 , and that the overall quenching of emission was closer to the smaller value.⁴¹ This would indicate a rapid redistribution of molecules that are in the discretely emitting levels over many different levels. The continuum emitting levels are strongly mixed with the 2A_1 ground state already by Douglas's mechanism, and it is unlikely that another ground state NO_2 will remove many quanta of energy from the NO_2^* , and therefore the σ_Q for NO_2 is less than might have been expected otherwise. However, the rate at which NO_2^* molecules will appear to be quenched

Table 7

<u>Gas</u>	<u>$k_Q \times 10^{11} \text{ (cm}^3\text{/part-sec)}$</u>	<u>$\sigma_Q \text{ (Å}^2\text{)}^{(1)}$</u>	<u>Ratio $\beta^{(2)}$</u>
He	2.5	1.93	1.25
Ar	3.2	5.96	1.52
N ₂	3.9	6.55	1.25
CO	4.8	8.06	--
NO	6.7	11.50	1.15
O ₂	3.6	6.30	1.06
CO ₂	7.7	14.71	0.96
N ₂ O	8.6	16.44	1.34
NO ₂	5.7	11.01	0.803

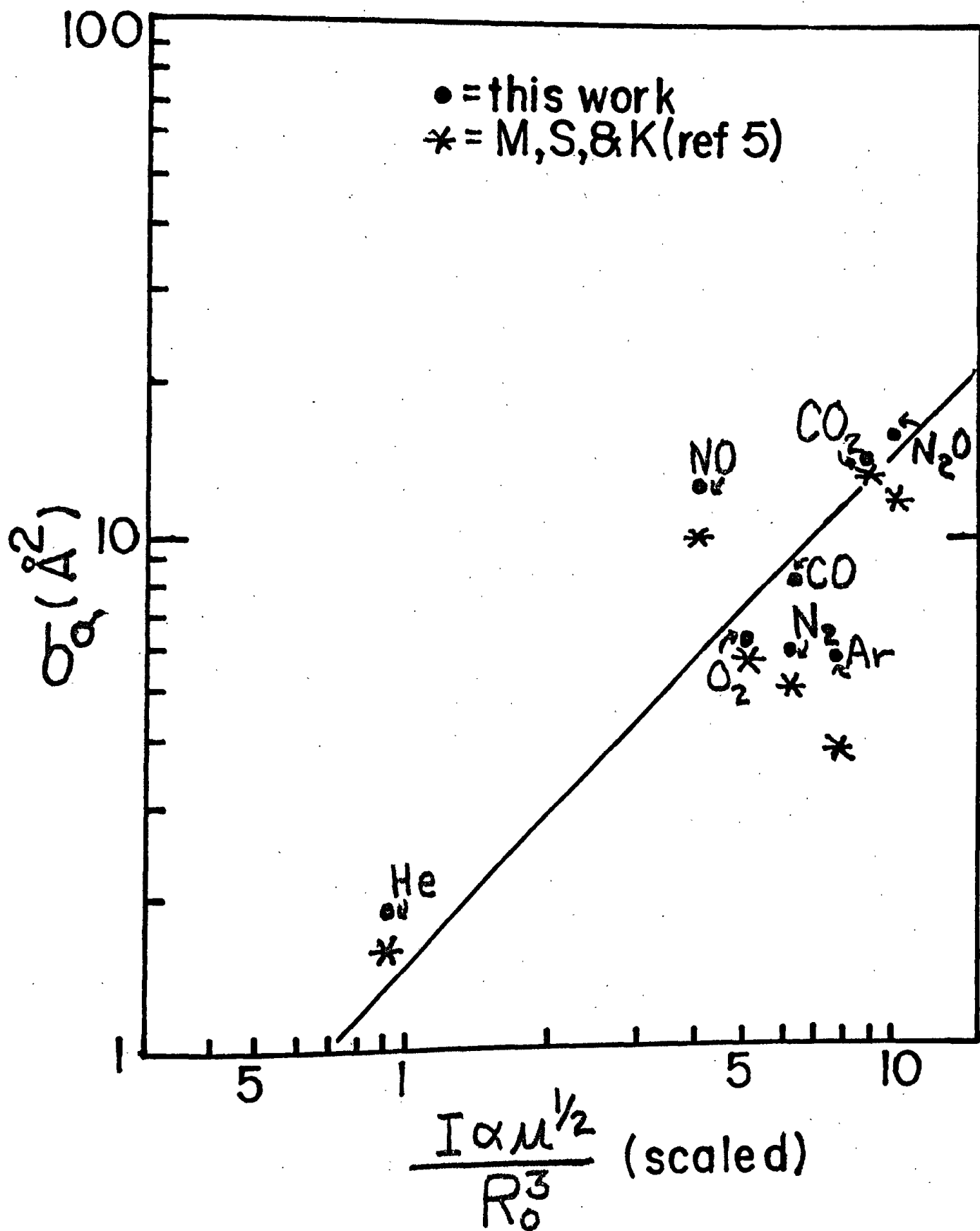
(1) The cross-sections σ_Q were calculated by using the relation

$$k_Q = (\pi d_{12}^2) \left(\frac{8kT}{\pi \mu} \right)^{1/2}$$

where $(\pi d_{12}^2) = \sigma_Q$, the quenching cross-section.

(2) The ratio β is the ratio of quenching cross-sections obtained in this work to those of Myers, Silver, and Kaufman.

Figure 20 Parametric Dependence of the Quenching Cross-Section Using
the Theory of Steinfeld and Selwyn



will be determined to a large extent by the rate at which they vibrationally relax to energy levels not detectable by the experimental apparatus. Care must be taken in the interpretation of the self-quenching constants for NO_2 obtained by various studies due to the simultaneous electronic and vibrational relaxation. Normally this problem would not be encountered, but the fairly long radiative lifetime and fairly large vibrational deactivation rates allow the two processes to occur on comparable time scales at the pressures used.

4.1.3 Self-Quenching of NO_2 at High Pressures

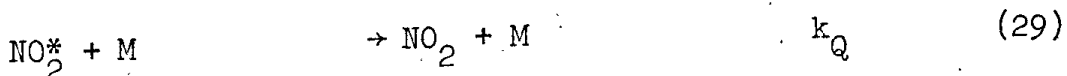
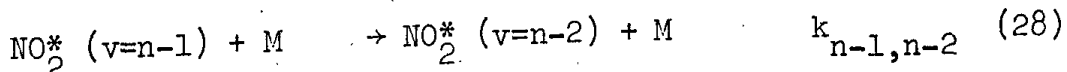
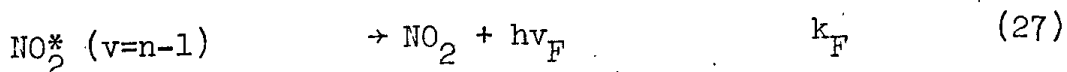
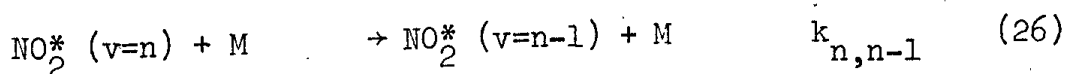
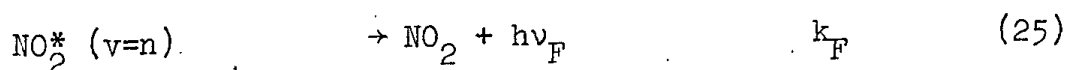
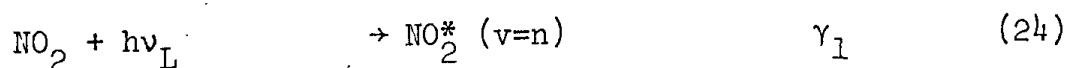
Under the experimental conditions used in this study an interesting phenomena was observed at higher pressures of NO_2 . The emission intensity did not simply decrease with time, but actually increased to a maximum before decaying. At even higher pressures a second maximum could be observed that peaked at longer times than the first maximum. The addition of other gases to NO_2 did not show this effect.

The general appearance of the time resolved emission was reminiscent of a consecutive reaction process wherein the secondary species are detected with a greater sensitivity than the initial species. The time to the first maximum decreased with increasing NO_2 pressure, and a plot of $1/\tau_{\text{max}}$ versus (NO_2) was essentially linear, but did show a fairly large non-zero intercept. The slope of the plot was about $4 \times 10^{-10} \text{ cm}^3/\text{part-sec}$. Using the consecutive mechanism mentioned earlier, the slope of the $1/\tau_{\text{max}}$ versus (NO_2) plot can be related to the bimolecular rate constants, but that leaves

us with one equation in two unknowns, so some means of relating the two rate constants is necessary to obtain estimates on their values.

A consecutive stepwise vibrational deactivation of NO_2^* has been used in the analysis of other experiments performed at fairly high NO_2 pressures using phase shift techniques.^{7,8} The phase shift between the excitation light modulation frequency and the fluorescence intensity frequency can be related to the lifetime of the excited state. However, in practice this method suffers from the fact that the data analysis requires assumption of a decay form (usually exponential), and that one does not observe directly the decay process itself. The results of Kaufman did, however, give an estimate of the vibrational deactivation rate constant of about $4 \times 10^{-10} \text{ cm}^3/\text{part-sec.}$ ⁷

A similar consecutive, stepwise deactivation scheme will be used here to explain the observed results and is given below:



etc. This mechanism ignores vibrational activation by collision and assumes that the radiative rate constant and electronic quenching rate constant are approximately independent of vibrational level. The quantum number v represents a general vibration (v_1, v_2, v_3) of the

2B_2 state. When a vibrational quantum is lost by collision it is not being specified which particular vibrational mode loses the quantum.

In order to even observe the maximum it must be true that $k_{n,n-1} > k_{n-1,n-2}$. If the vibrational relaxation occurs much faster than the electronic relaxation, which seems to be the case (otherwise the phenomena would be very difficult to observe), then we can neglect the effect of electronic quenching and write the reciprocal of the time to the first maximum as being;

$$\frac{1}{\tau_{\max}} = \left[\frac{k_{n,n-1} - k_{n-1,n-2}}{\ln\left(\frac{k_{n,n-1}}{k_{n-1,n-2}}\right)} \right] (M) \quad (30).$$

In order to extract values for $k_{n,n-1}$ and $k_{n-1,n-2}$ from the slope of the $1/\tau_{\max}$ versus (NO_2) plot, which has a value of $4 \times 10^{-10} \text{ cm}^3/\text{part-sec}$, a relationship between them must be assumed. There are two simple theoretical models that will be used, a harmonic oscillator model and a stepladder model.

In the harmonic oscillator model we are looking at the deactivation process as occurring in a single vibrational manifold. The levels are non-degenerate and the deactivation rate constant increases linearly with vibrational quantum number.⁵¹

In the stepladder model (used in the Rice-Ramsperger-Kassel theory of unimolecular reactions) there are assumed to be S effective modes of vibration which are strongly coupled and can transfer energy freely among these modes. For a given total vibrational energy there is an associated degeneracy factor. The deactivation rate constants are assumed to be proportional to the degeneracy of the final state to which the deactivation occurs.⁵²

The harmonic oscillator model is most valid near the bottom of an electronic potential well where the vibrational modes do act as normal modes and do not interact freely. The stepladder model is more valid as we go to higher vibrational levels and the anharmonicity becomes more pronounced allowing free flow of energy among the vibrational modes.

Table 8 shows the relationships among the relevant deactivation rate constants in terms of $k_{1,0}$, the value for the $v=1 \rightarrow v=0$ collisional deactivation, for both the harmonic oscillator and stepladder model. In Table 9 are presented the results of the calculations using these models. The $p_{1,0}$ value can be regarded as the probability per collision of inducing the $v=1 \rightarrow v=0$ transition. The reciprocal of this is $Z_{1,0}$, the collision number, which is the number of collisions required to deactivate $1/e$ of the molecules in the $v=1$ level. The other rate constants listed are the $k_{n,n-1}$ and $k_{n-1,n-2}$ values estimated using different values for n . In one case the $n=11$ value corresponds to the average number of quanta as counted from the ground state. This would be of importance if the 2B_2 and 2A_1 states are mixed, with the rapid deactivation occurring in the 2A_1 vibrational manifold. The $n = 3$ value is the average number of quanta from the bottom of the 2B_2 state and this would be of importance if there was little or no mixing of states.

As can be seen from this table, no matter which theory one uses, similar values are obtained. The rough estimates of 6 to $4 \times 10^{-10} \text{ cm}^3/\text{part-sec}$ for $k_{n,n-1}$ estimated from the rise time to maximum and of 5 to $3 \times 10^{-10} \text{ cm}^3/\text{part-sec}$ for $k_{n-1,n-2}$ from the

Table 8

<u>Harmonic Oscillator</u>	<u>Stepladder*</u>	
$k_{n,n-1}$	$= nk_{1,0}$	$[\frac{(n+s-2)!}{(n-1)!(s-1)!}]k_{1,0}$
$\frac{k_{n,n-1}}{k_{n-1,n-2}}$	$= \frac{n}{n-1}$	$(\frac{n+s-2}{n-1})$
$k_{n,n-1} - k_{n-1,n-2}$	$= k_{1,0}$	$[\frac{(n+s-3)}{(n-1)(s-2)}]k_{1,0}$

* Here s is the effective number of vibrational modes participating in the stepladder model.

Table 9

<u>For n = 11</u>	<u>S.L.M.</u> (a)	<u>H.O.M.</u> (a)	<u>Units</u>
$k_{11,10}$	4.35×10^{-16}	4.2×10^{-10}	$\text{cm}^3/\text{part-sec}$
$k_{10,9}$	3.63×10^{-10}	3.8×10^{-10}	$\text{cm}^3/\text{part-sec}$
$k_{1,0}$	6.6×10^{-12}	3.8×10^{-11}	$\text{cm}^3/\text{part-sec}$
$p_{1,0}$ (b)	0.0232	0.133	collision^{-1}
$z_{1,0}$	43	7.5	collisions
<u>For n = 3</u>			
$k_{3,2}$	11.0×10^{-10}	4.86×10^{-10}	$\text{cm}^3/\text{part-sec}$
$k_{2,1}$	5.52×10^{-10}	3.24×10^{-10}	$\text{cm}^3/\text{part-sec}$
$k_{1,0}$	1.84×10^{-10}	1.62×10^{-10}	$\text{cm}^3/\text{part-sec}$
$p_{1,0}$ (b)	0.643	0.566	collision^{-1}
$z_{1,0}$	1.55	1.76	collisions

(a) SLM = Stepladder Model with $s = 3$
 HOM = Harmonic Oscillator Model

(b) The $p_{1,0}$ was calculated using the hard-sphere collision rate constant of $2.86 \times 10^{-10} \text{ cm}^3/\text{part-sec}$ of Myers, Silver, and Kaufman.

decay time from the maximum provide independent support that the rate constants are of this magnitude. The most important result is that the vibrational relaxation is observed to be very fast, occurring at approximately every collision.

Collision numbers for various gases for vibrational to translational ($V \rightarrow T$) energy transfer range from as low as 1×10^3 to as high as 1×10^5 for such gases as CO_2 , N_2O , CS_2 , COS , and SO_2 . On the other hand when there is a resonant or near-resonant vibrational to vibrational ($V \rightarrow V$) energy transfer in polyatomics the collision numbers can be in the range of 3 to 122.⁵¹

The experimental result that the emission intensity maxima are brought about readily by addition of NO_2 but not by addition of other foreign gases implies a specific molecular interaction of NO_2^* with NO_2 . If the energy transfer were a simple $V \rightarrow T$ type then such a specific interaction would not be expected.

However, the $V \rightarrow T$ energy transfer process can be enhanced by larger intermolecular potentials. The dipole-dipole interactions of polar molecules and other long range interactions are known to increase the cross-sections for such inelastic scattering processes. For those gases which can form stable chemical compounds the effect of the bond-forming potential should be considered.

Since NO_2 can form a stable dimer, N_2O_4 , with a bond strength of 12.9 kcal/mole one might expect $V \rightarrow T$ transfer to be much more efficient than by an inert gas, so one might be led to believe that the process is a $V \rightarrow T$ transfer enhanced by the bond forming potential

of the N_2O_4 molecule. Nitric oxide, NO, showed no appreciably greater effect than any of the other gases used in the quenching studies and it can form a stable molecule, N_2O_3 , with an N-N bond strength of about 9.5 kcal/mole. However, the dependence of relative $p_{1,0}$ values on potential well depth can vary as $\exp[\Delta\epsilon/kT]$, where $\Delta\epsilon$ is the difference in well depths.⁵¹ This predicts that at room temperature NO_2 might be about 290 times more efficient than NO in the vibrational deactivation of NO_2^* . Recent results obtained by Golde and Kaufman on the quenching of vibrational chemiluminescence of NO_2^\ddagger formed in the $HO + O_3$ reaction indicates that NO_2 and NO are far more efficient than other gases used in their study, and attributed this to the chemical bond forming potential available to these molecules.⁵³ In this work at 6943\AA with the electronically excited NO_2 state, the vibrational effect will not be readily observed unless it is faster than electronic quenching, and $k_{Q,NO}^{(NO)}$ would be about 50 times greater than $k_{n,n-1}^{(NO)}$ if the $k_{n,n-1}^{(HO)}$ value is 290 times smaller than the $k_{n,n-1}^{(NO_2)}$ value.

A near-resonant $V \rightarrow V$ energy transfer is much more likely in a triatomic than in the diatomic, but it is impossible to say if this is occurring. At this time, due to the independent results of Golde and Kaufman, the enhanced $V \rightarrow T$ process seems more likely, but no differentiation between $V \rightarrow T$ and $V \rightarrow V$ transfer can be made.

The existence of a non-zero intercept in the $1/\tau_{\max}$ versus pressure plot could indicate that collisionless vibrational rearrangement is occurring simultaneously with fluorescence and collisional relaxation, and that one particular vibronic configuration is more likely to radiate than others. The vibrational energy in the excited state

could be redistributed among the vibrational modes such that emission is more readily seen after the redistribution than before. The data indicate that if this is so then the collisional deactivation rate equals the collisionless rearrangement rate at a pressure of 160 millitorr.

The second emission maximum may or may not be due to consecutive deactivation of the NO_2^* . If it is the NO_2^* ($v=n-2$) state then the sensitivity for its detection is larger than that for either the $v=n$ or $v=n-1$ states. The second maximum might also be due to a parallel deactivation of a different vibrational mode than for the first maximum. The decay time for the second maximum is pressure dependent with an apparent bimolecular decay constant in the neighborhood of $4 \times 10^{-11} \text{ cm}^3/\text{part-sec}$, which is about the value obtained for an apparent electronic deactivation rate constant from the low pressure data.

The emitting level of the second maximum may be the bottom level of the $^2\text{B}_2$ electronic state in which case the decay rate would be the electronic quenching rate. The fact that Sakurai and Broida saw 15 to 20\AA^2 cross sections for discrete emission features and a 0.9\AA^2 cross section for continuum features in addition with the previously discussed fact that $^2\text{B}_2$ emission is generally more discrete than $^2\text{B}_1$ emission indicates the possibility that the larger value is indeed the real value for the $^2\text{B}_2$ state.

The apparent quenching rate constant obtained in this work at 6943\AA at low pressures was $5.7 \times 10^{-11} \text{ cm}^3/\text{part-sec}$ (which may be complicated due to the vibrational relaxation). The apparent quenching

constant of the emitting state that comprises the second maximum is about $4 \times 10^{-11} \text{ cm}^3/\text{part-sec.}$ Since these values are for $\text{NO}_2^* (^2\text{B}_2)$ and since Sakurai and Broida observed a cross section corresponding to a quenching rate constant of 7×10^{-11} for the discrete (supposedly $^2\text{B}_2$) emission features, the conclusion that the $^2\text{B}_2$ state quenches at a rate about 10 times faster than the $^2\text{B}_1$ state is quite reasonable.

4.2 Two Photon Dissociation of NO_2

The photolysis experiments first performed by Gerstmayr, et al, showed that O_2 was produced as a result of the interaction of ruby laser radiation on NO_2 .²⁹ The experimental results obtained in this work that deal with O_2 formation were that the O_2 production as a function of NO_2 pressure was remeasured using a Pöckels cell to Q-switch the ruby laser, that the $\log(\text{O}_2 \text{ formed})$ versus $\log(\text{laser intensity})$ showed a slope of 2.0, and the isotopically substituted NO_2 did not photolyze randomly, but rather did show an isotope effect.

The direct dissociation of NO_2 into NO and O requires 71.8 kcal/mole, which is much greater than the 41.2 kcal/einstein which a ruby laser photon at 6943\AA provides. By simple energetics, the direct dissociation of NO_2 by light at 6943\AA cannot be done with the energy provided by one photon. The photodissociation reaction,



becomes possible for wavelengths shorter than 3945\AA .⁵⁴ Some dissociation is still observed to occur at a wavelength of 4070\AA , and it is proposed

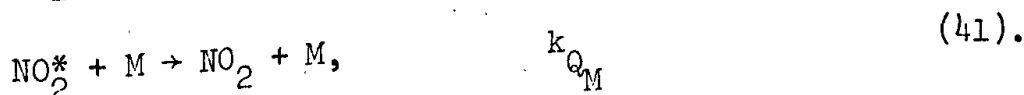
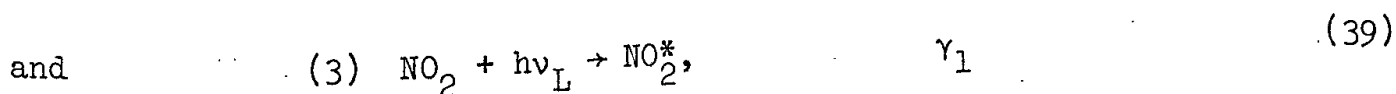
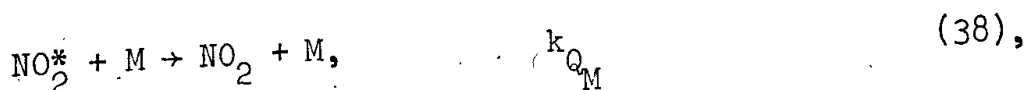
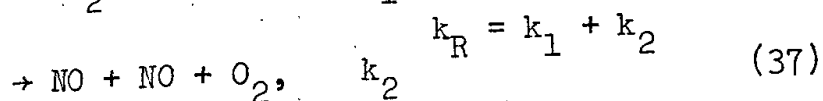
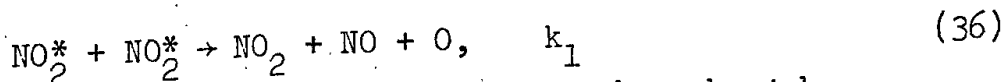
that this is due to the availability of the rotational and vibrational energy of the molecule.⁵⁵ At wavelengths of $4358\overset{\circ}{\text{A}}$ and greater no dissociation is found.

The reaction of an excited state with a ground state NO_2 ,



is energetically possible (requiring only a photon energy of 26 kcal/mole or a wavelength of $\sim 10,000\overset{\circ}{\text{A}}$), but this has never been observed in conventional photolysis (as mentioned above), and further, the results of the $\log \text{O}_2$ versus $\log I_L$ plot requires that at least two laser photons somehow participate in the O_2 formation process.

Three possible mechanisms consistent with an order for O_2 production with respect to laser intensity of 2.0 are (1) simultaneous absorption, (2) reaction of two excited states, and (3) consecutive absorption. These mechanisms are given below:



In all cases where an O atom is formed the fast reaction,



serves as a secondary step to form the O_2 .

In mechanism (1), the simultaneous absorption of two photons, the number of O_2 molecules formed will be equal to the number of O atoms produced, or half the number of photons absorbed by the simultaneous process. The O_2 formed by such a process can be estimated from the relation,

$$[\text{O}_2] = [\text{O}] = \frac{1}{2} \int_{\text{pulse}} I'_{\text{abs}} dt \quad (43),$$

$$\text{where,} \quad I'_{\text{abs}} = \delta I_L^2 n \ell \quad (44),$$

and δ is the two-photon absorption cross section in units of $(\text{cm}^4\text{-sec/molecule-photon})$, I_L is the incident laser intensity, n is the molecular particle density, and ℓ is the absorption cell length.⁵⁶ At an NO_2 pressure of 10 torr, and using a large two-photon cross section of $\delta = 10^{-49}$, the estimated O_2 formation after 5 laser pulses would be about 1.4×10^{15} particles O_2 compared with the measured value of $\sim 10^{17}$. Even assuming this large value for δ , this mechanism would contribute only $\sim 1\%$ of the observed O_2 formation.

Another factor against mechanism (1) being a major contribution is that O_2 formation levels off at higher pressures of NO_2 rather than remaining linear. This leveling off would be expected if there was a quenching step prior to the second photon absorption. However, in a simultaneous two photon process, the

lifetime of a "virtual" state is essentially limited by the uncertainty principle in that the uncertainty in energy of the state is approximately the energy of the photon creating it. A "virtual" state created by optical region photons will have a lifetime of about 10^{-15} seconds and cannot be collisionally quenched under these conditions.

Examining the kinetics of mechanism (2) we see that the O_2 formed will be given by,

$$[O_2] = k_R \int_0^{\infty} (NO_2^*)_t^2 dt \quad (45).$$

The differential equation for the loss of (NO_2^*) is given by,

$$\frac{d(NO_2^*)}{dt} = -[k_F(NO_2^*) + k_{QM}(NO_2^*)(M) + k_R(NO_2^*)^2] \quad (46).$$

Solving this equation and substituting into the above equation for O_2 allows one to estimate the value for the rate constant, k_R , as being in the neighborhood of $10^{-9} \text{ cm}^3/\text{part-sec}$ or about 10 times the gas kinetic rate constant. This is the rate at which fast ion-molecule reactions proceed wherein the polarization of the molecule by the ion allows long range electrostatic interactions to increase the reaction cross section. The triplet-triplet annihilation of biacetyl is one example of an excited-excited interaction that proceeds with approximately gas-kinetic cross section, but this involves only changes in electronic states, and not chemical bond rearrangement. It would seem unlikely that mechanism (2) accounts for the O_2 formation satisfactorily.

The consecutive absorption process proposed in mechanism (3) is entirely analogous to the photodissociation of phthalocyanine reported

by Porter prior to the initial work of Gerstmayr on NO_2 , and to subsequent two-step dissociations of NH_3 and BCl_3 reported by Letokhov and Rockwood, respectively.

The equations of interest are the following:



The differential kinetic equations for the above mechanism are given below:

$$\frac{d(\text{NO}_2^*)}{dt} = \gamma_1(\text{NO}_2) - [\gamma_2 + \lambda](\text{NO}_2^*) \quad (51),$$

$$\text{and} \quad \frac{+d(\text{O}_2)}{dt} \approx \frac{+d(\text{O})}{dt} = \gamma_2(\text{NO}_2^*) \quad (52).$$

Here λ is a pseudo-first order rate constant that is the sum of the fluorescence rate constant and the sum of the products of quenching rate constants and pressure,

$$\lambda = k_F + \sum_{i=1}^N k_{Q_i}(\text{M}_i) \quad (53).$$

In the case of NO_2 , k_F is negligible in comparison with quenching at the pressures used. The number of O_2 molecules formed will be equal to the number of O atoms formed in the two-step photodissociation since they react rapidly with NO_2 to form O_2 and NO. The kinetic modeling of a two-step process is given in Appendix I. The solution to this problem for the special conditions used in this work given the total amount of

O_2 formed by a laser pulse as being,

$$(O_2) = \frac{\gamma_1 \gamma_2 (NO_2)^T}{(\gamma_2 + \lambda)} \left[1 + \frac{(e^{-(\gamma_2 + \lambda)T} - 1)}{(\gamma_2 + \lambda)T} \right] \quad (54),$$

where T is the duration of the laser pulse, assumed to be a square wave pulse for purposes of calculation, and γ_1 and γ_2 are the first order excitation rate constants for the first and second excitations respectively. These γ 's are the products of laser photon flux and absorption cross section.

Expanding the exponent in the above equation and keeping the first three terms gives the approximation,

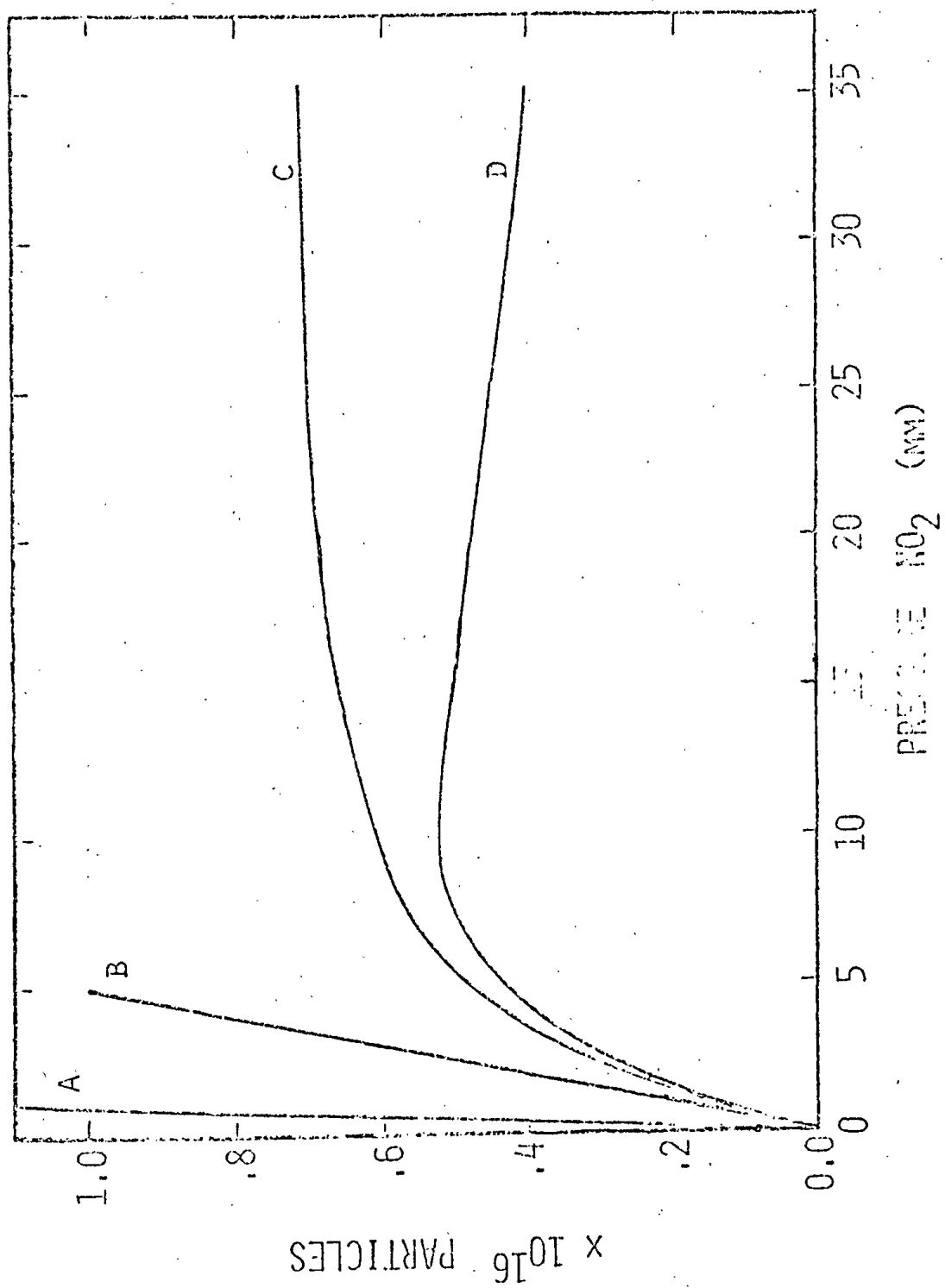
$$(O_2) \approx \frac{\gamma_1 \gamma_2 (NO_2)^T^2}{2} \quad (55).$$

This shows that the I_L^2 dependence for O_2 formation is to be expected in the limit of low quenching and when γ_2 is not so large that all the excited states, NO_2^* , are further excited and dissociated by the second photon.

Calculated curves showing (O_2) as a function of (NO_2) for one laser pulse using this works measured quenching constants and other known parameters are shown in Figure 21. Curves are shown for (NO_2^*) as a function of (NO_2) and for (O_2) as a function of (NO_2) assuming no quenching, quenching, and quenching along with dimerization of NO_2 to N_2O_4 .

As can be seen, these theoretical curves are in good agreement with the experimental data. The only unknown parameter is the value for the second absorption coefficient. The value used in calculating the above curves is calculated below.

Figure 21 Calculated O_2 Production Curve for One Laser Pulse Using
the Consecutive Absorption Model



The second absorption coefficient can be estimated in the following way. Knowing the number of NO_2^* molecules formed during the course of the laser pulse (without quenching), to be given by,

$$(\text{NO}_2^*)_{\text{pulse}} = \gamma_1 (\text{NO}_2) T \quad (56),$$

where T is the pulse duration, we can derive an expression for the fraction of NO_2^* that go on to form O_2 molecules as a function of γ_2 . Using the above equations (54) and (56), we can see that this fraction is given by,

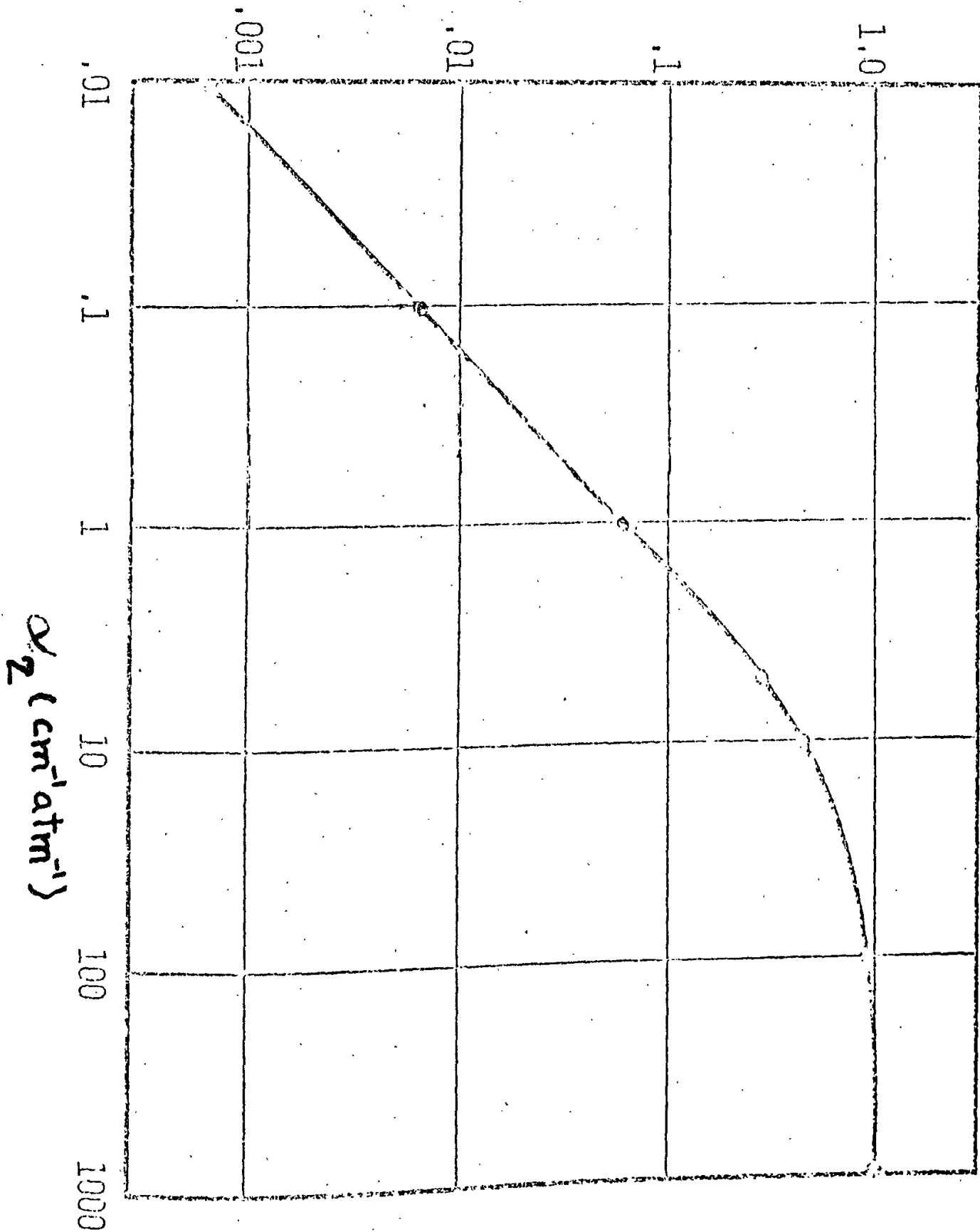
$$\frac{(\text{NO}_2^*) \rightarrow (\text{O}_2)}{(\text{NO}_2^*)} = \frac{(\text{O}_2)}{\gamma_1 (\text{NO}_2) T} = \left[1 + \frac{(e^{-\gamma_2 T} - 1)}{\gamma_2 T} \right] \quad (57),$$

in the limit of zero quenching. This is the ratio of the tangent of the (O_2) versus (NO_2) curve at zero NO_2 pressure to the slope of the (NO_2^*) versus (NO_2) curve; this ratio is an experimentally determinable quantity. Plotting out equation (57) as shown in Figure 22 allows a graphical estimate to be made for γ_2 , and therefore for the second absorption coefficient.

The value for the first absorption coefficient in the neighborhood of the laser line is about $0.15 \text{ cm}^{-1} \text{ atm}^{-1}$ ($= 6 \times 10^{-21} \text{ cm}^2/\text{molecule}$). Using Beer's Law, the number of NO_2^* formed during one pulse throughout the entire photolysis cell volume is about $7 \times 10^{16} \text{ NO}_2^*$ for a pressure of 7.5 torr of NO_2 . The number of O_2 molecules formed (for zero quenching) would correspond to 2×10^{16} particles of O_2 per pulse. The fraction of NO_2^* that go on to form O_2 is therefore about 28% under the present photolysis conditions. Graphical analysis using Figure 22 gives an estimate for the second

Figure 22 Log of the Fraction of NO_2^* Molecules Forming O_2 Versus
the Log of the Second Absorption Coefficient

$$(O_2) / \gamma_1(NO_2)T$$



absorption coefficient of $3.3 \text{ cm}^{-1} \text{ atm}^{-1}$ ($= 1.3 \times 10^{-19} \text{ cm}^2/\text{particle}$).

This estimated γ_2 value was used as the γ_2 value in the calculated O_2 production curves of Figure 21.

The isotope effect experiments performed with a mixture of normal O-16 and O-18 isotopically substituted NO_2 gave some interesting results. The mixture ($2/3 \text{ }^{14}\text{N}^{16}\text{O}_2 - 1/3 \text{ }^{14}\text{N}^{16}\text{O}^{18}\text{O}$) when photolyzed under sunlight for 25 minutes produced O_2 which had an isotope ratio for $^{16}\text{O}^{18}\text{O}/^{16}\text{O}_2$ of about 0.4 (see Table 5). This is to be expected if the photodissociation is random, that is, isotopically non-selective. The number of initially formed O atoms will be $1/6\text{-}^{18}\text{O}$ and $5/6\text{-}^{16}\text{O}$. These will then react randomly with the NO_2 to form O_2 . The fractions of O_2 formed will be given by the following:

$$\begin{array}{ll}
 1/6\text{-}^{18}\text{O} \times 1/6\text{-}^{18}\text{O} \text{ (from } ^{16}\text{O}^{18}\text{O}) & = 1/36 \\
 1/6\text{-}^{18}\text{O} \times 5/6\text{-}^{16}\text{O} \text{ (from } ^{16}\text{O}_2 \text{ and } ^{16}\text{O}^{18}\text{O}) & = 5/36 \\
 5/6\text{-}^{16}\text{O} \times 1/6\text{-}^{18}\text{O} \text{ (from } ^{16}\text{O}^{18}\text{O}) & = 5/36 \\
 5/6\text{-}^{16}\text{O} \times 5/6\text{-}^{16}\text{O} \text{ (from } ^{16}\text{O}_2 \text{ and } ^{16}\text{O}^{18}\text{O}) & = 25/36 \\
 \text{Fraction Sum Total} & = 1.000
 \end{array}$$

The randomly photolyzed mixture would give $1/36\text{-}^{18}\text{O}_2$, $10/36\text{-}^{16}\text{O}^{18}\text{O}$, and $25/36\text{-}^{16}\text{O}_2$. The ratio of $m/e = 34(^{16}\text{O}^{18}\text{O})$ to $m/e = 32(^{16}\text{O}_2)$ will be $(10/25)$ or 0.400, which was the experimentally observed ratio for the sunlight photolysis.

With the initial isotope ratios chosen, it can be shown that the ratio R of $m/e = 34$ to $m/e = 32$ is equal to

$$R = 0.2 + (\alpha_2 / 4\alpha_1 + \alpha_2) \quad (58),$$

when photolysis is non-random, and α_1 is the absorption coefficient for

the $^{14}\text{N}^{16}\text{O}_2$ species and α_2 is the absorption coefficient for the $^{14}\text{N}^{16}\text{O}^{18}\text{O}$ species. From this the relative absorption coefficients can be seen to be given by the relation,

$$\frac{\alpha_2}{\alpha_1} = \left(\frac{4R - 0.8}{1.2 - R} \right) \quad (59).$$

Values of (α_2/α_1) are calculated and given in Table 10. In spite of what should be no more than a 10 to 20% error in the measurement of R, the (α_2/α_1) values vary by more than a factor of 10. This variation can be attributed to the fact that the NO_2 spectrum consists of very densely packed, but nevertheless narrow absorption lines. As mentioned in the experimental section, a 2°C shift from room temperature will cause a 0.138\AA shift in the ruby laser wavelength or about twice the spectral breadth of the ruby line. The width of an NO_2 absorption line can be calculated from the relation for Doppler-broadening as being,

$$\Delta\lambda = 7.17 \times 10^{-7} \sqrt{\frac{T}{M}} \lambda_0 \quad (60),$$

where T is in $^\circ\text{K}$ and M is the molecular mass in AMU's. This gives a Doppler breadth of 0.0125\AA for NO_2 at 293°K and $\lambda_0 = 6943\text{\AA}$. Even a relatively small wavelength shift can cause the laser to overlap different absorption lines and/or to cease exciting other lines.

The choice of ^{18}O as the isotopic substituent was made because the scrambling reaction,



is known to proceed very slowly in the dark and would not interfere with mass-spectral measurements on the time scale used.⁵⁷ The scrambling of oxygen isotopes within the O_2 system (which occurs very rapidly in the

Table 10

Calculated (α_2/α_1) Ratios from Isotope Data

<u>Expt. #</u>	<u>R*</u>	<u>(α_2/α_1)</u>	<u>Comments</u>
1	0.546	2.11	Laser 5x
2	0.471	1.5	Laser 5x
3	1.10	36	Laser 5x
4	0.398	1.00	Sunlight

* The theoretical R value for the isotope mixture used should be $R = 0.400$, corresponding to an $(\alpha_2/\alpha_1) = 1.000$.

presence of O atoms or O₃) would tend to decrease the $^{16}\text{O}^{18}\text{O}/^{16}\text{O}_2$ ratio since more of the ^{18}O would be in the form of $^{18}\text{O}_2$. On the other hand, the reaction



is known to proceed with extreme rapidity; the time it would take for about 1/e of any initially formed ^{15}NO to scramble being 36 microseconds at an NO_2 pressure of 10 torr.⁵⁷ The spectrum of $^{15}\text{NO}_2$ is known to exhibit marked isotope shifts, so a selective excitation would perhaps be easier for this species, but the speed of the scrambling reaction prohibits the use of the two-step photodissociation as a means of separation of ^{15}N .⁵⁸ Conceivably, ^{18}O could be separated, but a much higher degree of temperature control and stability than the present laser system possesses is required.

4.3 Multiphoton Induced Fluorescence

The fact that emission is observed in the spectral region observed of 4,000 to 4,400 Å necessarily implies the pooling of energy of more than one ruby laser photon in some manner, either by consecutive absorptions, by collisional interactions of excited states, or by some other type of mechanism.

The "blue" emission is found to increase more or less linearly with pressure at lower pressures, peak at about (NO_2) of 30 torr and then decrease with NO_2 pressure. This fall-off is probably due to self absorption of emitted light, since the absorption coefficient of NO_2 is about 2 orders of magnitude higher in this spectral region than at the 6943 Å line.

The lifetime of the emission is found to be collisionally-limited, with a collisional quenching constant of about 2.5×10^{-11} cm³/part-sec. This is in line with the quenching constants for NO₂^{*} found by Hg-lamp 4358Å^o excitation as studied by Myers, et al.⁵

Nitrogen dioxide does not fluoresce when excited at wavelengths below 4,000Å^o, but rather predissociates. Busch and Wilson have studied the photodissociation of NO₂ using a frequency doubled pulsed ruby laser at $\lambda = 3472\text{Å}^{\circ}$ and estimate the lifetime of the state excited to be about 2×10^{-13} seconds.⁵⁹ The angular distribution of products allowed them to identify it as a ²B₂ state, probably the same state responsible for the absorption extending into the infra-red. An independent estimate of the lifetime of NO₂^{*} at energies above the dissociation limit obtained by high pressure photolysis measurements of NO₂ also gave a value of 2×10^{-13} seconds.⁶⁰ Other higher electronic levels of NO₂ are not observed in emission.⁶¹

Taking into account the spectral region observed, the experimentally observed lifetime (40 to 140 nanoseconds), and other known spectroscopic data, it must be concluded that the observed species is an NO₂^{*} formed below the dissociation limit.

Perhaps the most interesting piece of experimental data is that slope of the $\log I_F$ versus $\log I_L$ plot changes from 3.0 for low pressures to a limiting value of 2.0 at higher pressures. Apparently, the emission is due to contributions from a two-photon process that contributes to a greater extent at high pressures and from a three-photon process that predominates at lower pressures. Formulating the emission

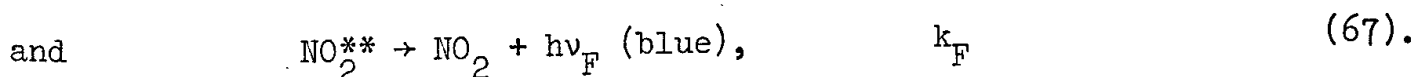
intensity as a sum of two and three photon processes,

$$I_F = C_1 I_L^2 + C_2 I_L^3 \quad (63),$$

and plotting I_F/I_L^2 as a function of I_L should give straight lines of slope C_2 and intercept C_1 . The slope to intercept ratio (C_2/C_1) will be a relative measure of the three photon to the two photon process for the given pressure of NO_2 . Calculating (C_2/C_1) as a function of pressure showed it to be inversely proportional to pressure. The two photon process therefore depends on pressure to one order higher than the three photon process.

If the pressure dependence at low pressures is linear, as it seems to be, then this would mean that the three photon process $\propto P$ and the two photon process $\propto P^2$. It is necessary to keep this in mind as well as the fact that the emitting NO_2^* must be below the dissociation limit when considering possible mechanistic interpretations of the results.

One possible mechanism that would explain a I_L^2 laser dependence and a P^2 pressure dependence is the following:

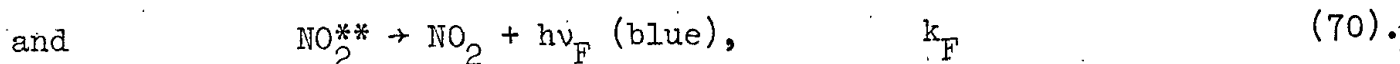


It can be seen from this that $I_F \propto I_L^2 (\text{NO}_2)^2$.

Since twice the laser energy corresponds to $28,803 \text{ cm}^{-1}$ and the dissociation limit is at $25,132 \text{ cm}^{-1}$, some amount of energy $\Delta E (\geq 3,671 \text{ cm}^{-1})$

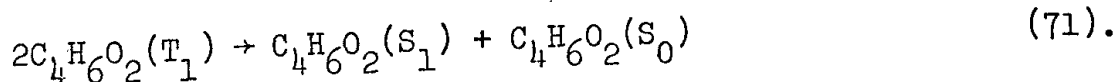
must be removed from the NO_2^* prior to the second excitation step. This would require a multiquantum deactivation, which are generally of much lower probability per collision than single quantum deactivations. However, this blue emission process does not proceed with a high overall efficiency anyways, and such a deactivating step seems entirely reasonable.

Another possible mechanism is the interaction of two excited states as shown below:



Here $I_F \propto I_L^2 (\text{NO}_2)^2$ and this mechanism would show the same behavior as collisional deactivation. In looking at the variation of lifetime with laser intensity at fixed NO_2 pressure, no τ_{obs} dependence on I_L is found. This might be expected at low pressures since the $\text{NO}_2^* - \text{NO}_2^*$ interaction is less likely to be a major contribution to the emission. At the high pressures where it might be expected, if that mechanism were operative, the lifetime measurements become less meaningful as $\tau_{\text{obs}} \rightarrow T$ (the laser pulse duration); a small change in τ_{obs} would be very difficult to observe.

The excited-excited interaction is analogous to the triplet-triplet of biacetyl observed by Calvert and co-workers,⁶²



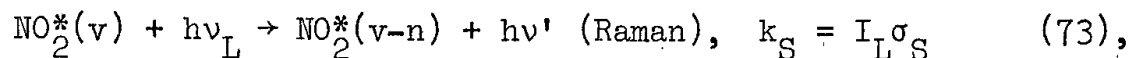
Whereas this type of interaction could not account for the O_2 formation observed in the two-photon dissociation of NO_2 , it can account for the

blue emission since even a small rate constant, k_{ET} , for the energy transfer process would allow creation of enough NO_2^{**} for observation of the light emission.

At this time it is difficult to distinguish on the basis of experimental evidence or theoretical arguments as to which of the two proposed mechanisms accounts for the I_L^2 contribution to the observed blue fluorescence.

Another non-linear I_L^2 process that could give rise to a "blue" emission is the hyper-Raman effect.⁶³ In this process the first photon raises the molecule to a virtual state, and the second photon raises the molecule to a second virtual state from which the third photon emerges as a scattered or emitted photon. This third photon can connect with a vibrational level different than the initial state giving rise to a shift, so that it is of less energy than $2h\nu_L$ but greater energy than $h\nu_L$. However, if this were a substantial contribution to the I_L^2 process one would expect the I_L^2 pressure dependence to be the same as for the I_L^3 process (which it is not). Also, since the second virtual state (or real state if one happens to be in the neighborhood) determines the lifetime of the emission and this is expected to be short ($< 10^{-13}$ sec) then the emission would have to follow the time dependence of the laser pulse (which it does not). On this basis, the hyper-Raman effect is not considered to be a major contributing process in these experiments.

The only mechanism that seems to satisfactorily account for the I_L^3 dependent term is given below:



This mechanism gives an I_L^3 laser dependence and a first order NO_2 pressure dependence. The required deactivating step is not a collision, but rather is an anti-Stokes Raman scattering off of the NO_2^* intermediate removing n effective vibrational quanta. Consideration of the magnitude of the NO_2 and NO_2^* vibrational quanta indicates that some combination of at least 3 quanta must be removed in the scattering process if the final NO_2^{**} formed by the second excitation step is to be below the dissociation limit of NO_2 .

In one way of looking at the scattering process, the incident photon of frequency ν_0 raises the molecule to an intermediate state from which it rapidly deactivates by emitting the scattered photon of frequency ν_S . If $\nu_0 = \nu_S$, then we have Rayleigh scattering, if $\nu_0 > \nu_S$, then we have what is called Stokes scattering, and if $\nu_0 < \nu_S$ we have an anti-Stokes scattering. In studying Raman scattering off of ground state molecules Stokes-shifted lines are generally of much greater intensity than anti-Stokes lines due to the difference in level populations at thermal equilibrium as required by Boltzmann's energy distribution law. However, in scattering off of an excited state, the molecule can be placed in a high vibrational level and the probabilities for either Stokes or anti-Stokes scattering off of a given vibrational level are approximately equal.

If the intermediate state to which the molecules is raised is near an energy level of the molecule, then the cross section for the scattering process is greatly enhanced, becoming larger as the energy difference $\rightarrow 0$. This is usually referred to as resonance Raman scattering even though it is usually a near resonance rather than a true resonance. In the case of scattering off of NO_2^* with ruby laser light there are predissociating ${}^2\text{B}_2$ levels present at the energy that would correspond to the intermediate state, as has been shown by the experiments of Busch and Wilson. Since these vibronic levels have been smeared out into a continuum by the predissociation, it seems likely that there will be an enhancement of the scattering cross section due to resonance effects.

Taking into account the filter combination transmittance, photomultiplier gain, a geometric factor (assuming an inverse square intensity diminution along with no effective diffusion of the radiators from the beam path), and the total signal in coulombs (estimated by integrating a decay curve) an order of magnitude quantum efficiency for the overall process,

$$\text{NO}_2^{**} \rightarrow \text{NO}_2 + h\nu_F, \quad \phi_F \quad (76),$$

of $\phi_F \approx 5 \times 10^{-10}$ for an NO_2 pressure of 11 torr was estimated. This quantum efficiency can be related to the scattering process as being,

$$\phi_F = A \left[\frac{k_F}{k_F + k_Q(\text{NO}_2)} \right] I_L \sigma_S \quad (77),$$

where A is a factor depending on laser pulse duration and intensity and is estimated to be about 0.25. Using $k_F = 2.7 \times 10^4 \text{ sec}^{-1}$ and a k_Q of

$4 \times 10^{-12} \text{ cm}^3/\text{part-sec}$, an estimate for the scattering cross-section of $\sigma_S = 5 \times 10^{-26} \text{ cm}^2/\text{part}$ is obtained.

This is a fairly large Raman scattering cross-section and indicates that a resonance effect may be occurring. Resonance Raman scattering off of ground state NO_2 molecules involving discrete levels near the intermediate state has been observed previously, with an estimated σ_S in the neighborhood of 10^{-24} to $10^{-25} \text{ cm}^2/\text{part}$.^{64,65} One consequence of the resonance effect is that some overtones and combinations (symmetric ones) are of nearly identical intensity with the fundamental bands.⁶⁴

Since $C_2 \approx C_1$ at an O_2 pressure of 25 torr and a relative laser intensity of $I_L = 1.0$, an estimate of the rate constant value for the deactivating step of $k_D \approx 2 \times 10^{-17} \text{ cm}^3/\text{part-sec}$, or for the excited interaction step of $k_{ET} \approx 7 \times 10^{-16} \text{ cm}^3/\text{part-sec}$ can be made. Either of these are entirely reasonable rate constants for the processes proposed.

The calculated ϕ_F depends naturally on the second absorption coefficient whose actual value may differ from the one estimated from the O_2 formation studies but it should not differ by many orders of magnitude.

CONCLUSIONS

The studies performed in this work on NO_2 using the pulsed ruby laser exciting at a wavelength of $6943\overset{\circ}{\text{A}}$ have yielded information on the dynamic processes occurring in NO_2 under the influence of high laser light intensities. These results have been most easily discussed in terms of (a) processes occurring as a result of absorption of one photon (i.e., fluorescence, quenching, and vibrational deactivation), (b) the two-photon induced dissociation of NO_2 occurring via a consecutive absorption mechanism, and (c) the multiphoton induced emission processes occurring by both the two and three photon mechanisms. A summary of the conclusions reached as a result of this work is given below.

A. The fluorescence studies have yielded the following information:

(1) The radiative lifetime is similar in magnitude to most others obtained experimentally, no unusually short-lived decays being observed. This may be due to the fact that τ_0 for the ${}^2\text{B}_2$ state actually is in the order of 40 microseconds, or that what would be a shorter lived state is lengthened by mixing with the ground state.

(2) The quenching constants for gases other than NO_2 are similar to those obtained by Myers, Silver, and Kaufman with $4358\overset{\circ}{\text{A}}$ excitation. However, if their values are adjusted using a more recent lifetime for NO_2^* formed in this spectral region (their experiments measured $k_Q\tau_0$ not k_Q directly) then the quenching

constants obtained here are about a factor 1.7 higher in general. This is understandable since excitation in their spectral region will excite both the 2B_2 state and the less readily quenched 2B_1 state.

(3). The vibrational deactivation of NO_2^* (2B_2) was directly observed and occurs at approximately the gas kinetic collision rate for NO_2 . The deactivation most likely occurs via a $V \rightarrow T$ energy transfer enhanced by the bond forming potential of N_2O_4 .

(4) The electronic quenching constant for NO_2^* (2B_2) formed below the (0,0,0) level of the 2B_1 state may very well be in the order of $5 \times 10^{-11} \text{ cm}^3/\text{part-sec}$ rather than the $4 \times 10^{-12} \text{ cm}^3/\text{part-sec}$ found by Sakurai and Broida.

(5) These results lead to a clarification of the dynamics of NO_2^* formed by optical excitation. When one excites NO_2 electronically above the (0,0) level of the 2B_2 state but below the (0,0) level of the 2B_1 state the quenching behavior shows a rate constant approximately 1/10 the gas kinetic rate. The transition ${}^2B_2 \rightarrow {}^2A_1$ is collisionally induced and since the 2B_2 and 2A_1 states do not mix well there is no way for the molecule to easily "wander back" into the 2B_2 state and emit light. However, above the (0,0) level of the 2B_1 state where there is absorption occurring simultaneously to both the 2B_1 and 2B_2 states, there are two types of quenching. Apparently, the more discrete emission features (occurring from 2B_2 levels) are quenched at about 1/10 the gas kinetic rate, while the continuum and overall emission is quenched at about 1/100 the gas kinetic rate. A possible

mechanism is that the ${}^2B_2 \rightarrow {}^2A_1$ collision induced transition is fairly rapid and permanent (once an $NO_2^* ({}^2B_2)$ is lost it cannot be reformed), but since the intramolecular transition ${}^2B_1 \leftrightarrow {}^2A_1$ occurs as a result of both collisional and collisionless processes the excited state, as such, is not lost, but eventually shows up again as an $NO_2^* ({}^2B_1)$. The observed collisional loss rate is the rate of deactivation to a level below the (0,0) level of the 2B_1 state. This could occur directly, converting a large portion of the excitation energy into translational and/or vibrational-rotational energy, or by a stepwise vibrational deactivation. As shown by the direct observation of the first and second emission maxima, this vibrational cascading occurs at a very rapid rate.

B. The results of the O_2 formation studies show that the O_2 is clearly formed by a two-photon process and that the consecutive absorption mechanism is the only one that can consistently explain all the data. An estimate for the second absorption step (to the dissociation continuum) of $3.3 \text{ cm}^{-1} \text{ atm}^{-1}$ could be made. The calculated curves show that the quenching of the intermediate NO_2^* must be taken into account to explain the observed leveling off of O_2 produced with increasing NO_2 pressure. The calculations performed in Appendix I for a more general two-step photoreaction show that if $\nu_1 \neq \nu_2$ then a specific delay time for product optimization between the absorption of the first and second photons exists, and can be estimated given specific experimental parameters.

The isotope effect experiments show promise for application to the separation of the ${}^{18}O$ isotope if a more wavelength stable arrangement

is used, but the results obtained to date are not quantitatively reproducible enough to accurately estimate separation factors.

C. The observation of a blue emission indicates the existence of multiphoton induced phenomena. The data is consistent with two pathways. The first shows an I_L^2 dependence and is a consecutive absorption requiring an intermediate collisional deactivation of the NO_2^* . The second shows an I_L^3 dependence and is also a two photon consecutive absorption, but requires instead an anti-Stokes scattering collision to deactivate the NO_2^* intermediate. This scattering step introduces another order in the laser intensity dependence and an I_L^3 dependence results.

The direct observation and spectral resolution of such excited state Raman scattering has the potential of yielding information on excited state structure presently unobtainable by other methods.

LITERATURE CITED

1. Norrish, R. G., J. Chem. Soc., 1611 (1929).
2. Baxter, W., J. Amer. Chem. Soc., 52, 3920 (1930).
3. Heil, O., Z. Physik, 77, 563 (1932).
4. Neuberger, D. and Duncan, A. B. F., J. Chem. Phys., 22, ~~1693~~ (1959).
5. Myers, G., Silver, D., and Kaufman, F., J. Chem. Phys., 44, 718 (1966).
6. Dixon, J. K., J. Chem. Phys., 8, 157 (1940).
7. Keyser, L., Levine, S., and Kaufman, F., J. Chem. Phys., 54, 355 (1971).
8. Schwartz, S. and Johnston, H., J. Chem. Phys., 51, 1286 (1969).
9. Sackett, P. B. and Yardley, J. T., J. Chem. Phys., 57, 152 (1972).
10. Sidebottom, H. W., Otsuka, K., Horowitz, A., Calvert, J. G., Rabe, B. R., and Damon, E. K., Chem. Phys. Lett., 13, 337 (1972).
11. Hardwick, J. L. and Brand, J. C. D., Chem. Phys. Lett., 21, 458 (1973).
12. Brand, J. C. D., Hardwick, J. L., Pirkle, R. J., and Seliskar, C. J., Can. J. Phys., 51, 2184 (1973).
13. Reeves, R. R., Harteck, P., and Chace, W. H., J. Chem. Phys., 41, 764 (1964).
14. Appelbaum, D., Harteck, P., and Reeves, R. R., Photochem. and Photobiol., 4, 1003 (1965).
15. McKenzie, A. and Thrush, B. A., Chem. Phys. Lett., 1, 681 (1968).
16. Becker, K. H., Groth, W., and Thran, D., Chem. Phys. Lett., 6, 583 (1970).
17. Fontijn, A., Sabadell, A., and Ronco, R., Anal. Chem., 42, 575 (1970).
18. Leighton, P. A., Photochemistry of Air Pollution, Academic Press, New York (1961).
19. Jones, I. T. N. and Bayes, K. D., J. Chem. Phys., 59, 3119 (1973).
20. Foote, C. S., Accounts of Chem. Res., 1, 104 (1968).

21. Goeppert-Mayer, M., Ann. Physik, 9, 273 (1931).
22. Pao, Y. H. and Rentzepis, P. M., Appl. Phys. Lett., 6, 93 (1965).
23. Porter, G., Nature (London), 215, 502 (1967).
24. Speiser, S. and Kimel, S., J. Chem. Phys., 51, 5614 (1969).
25. Wang, C., and Davis, L., J. Chem. Phys., 62, 53 (1975).
26. Porter, G. and Steinfeld, J. I., J. Chem. Phys., 45, 3456 (1966).
27. Ambartzumian, R., Letokhov, V., Makarov, G., and Puretzki, K., JETP Lett., 15, 709 (1972).
28. Rockwood, S. and Rabideau, S., Talk presented at the 8th IQEC, San Francisco (1974).
29. Gerstmayr, J., Harteck, P., and Reeves, R., J. Phys. Chem., 76, 474 (1972).
30. Wunsch, L., Neusser, H., and Schlag, E., Chem. Phys. Lett., 31, 433 (1975).
31. Wunsch, L., Neusser, H., and Schlag, E., Chem. Phys. Lett., 32, 210 (1975).
32. Hänsch, T., Lee, S., Wallenstein, R., and Wieman, C., Phys. Rev. Lett., 34, 307 (1975).
33. Harris, L. and Churney, K., J. Chem. Phys., 47, 1703 (1967).
34. Lengyel, B., Introduction to Laser Physics, John Wiley and Sons, Inc., New York (1966).
35. Stevens, C. G., Swagel, M. W., Wallace, R., and Zare, R. N., Chem. Phys. Lett., 18, 465 (1973).
36. Abe, K., Myers, F., McCubbin, T. K., and Polo, S. R., J. Mol. Spect., 50, 413 (1974).
37. Butler, S., Kahler, C., and Levy, D., J. Chem. Phys., 62, 815 (1975).
38. Sackett, P. B. and Yardley, J. T., Chem. Phys. Lett., 9, 612 (1971).
39. Solarz, R., Levy, D., Abe, K., and Curl, R. F., J. Chem. Phys., 60, 1158 (1974).
Solarz, R., Butler, S., Levy, D., J. Chem. Phys., 58, 5172 (1975).
40. Abe, K., J. Mol. Spect., 48, 395 (1973).

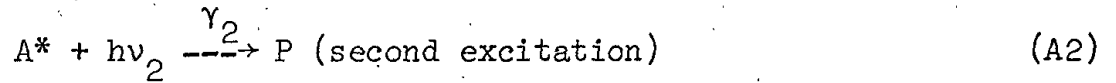
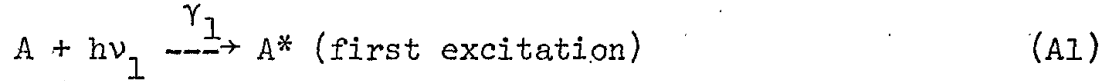
41. Sakurai, K. and Broida, H. P., J. Chem. Phys., 50, 1404 (1969).
42. Douglas, A. E., J. Chem. Phys., 45, 1007 (1966).
43. Messiah, A., Quantum Mechanics Vol. II, John Wiley and Sons, Inc., New York (1958).
44. Keyser, L. F., Kaufman, F., and Zipf, E. C., Chem. Phys. Lett., 2, 523 (1968).
45. Bixon, M. and Jortner, J., J. Chem. Phys., 48, 715 (1968).
46. Gardner, P. J., Chem. Phys. Lett., 4, 167 (1969).
47. Schwartz, S. E. and Senum, G. I., Chem. Phys. Lett., 32, 569 (1975).
48. Steinfeld, J. J., Accts. of Chem. Res., 4, 313 (1970).
49. Rössler, F., Z. Physik, 96, 251 (1935).
50. Selwyn, J. E. and Steinfeld, J. I., Chem. Phys. Lett., 4, 217 (1969).
51. Stevens, B., Collisional Activation in Gases, Pergamon Press, Oxford (1967).
52. Forst, W., Theory of Unimolecular Reactions, Academic Press, New York (1973).
53. Golde, M. and Kaufman, F., Chem. Phys. Lett., 29, 480 (1974).
54. Calvert, J. G. and Pitts, J. M., Photochemistry, John Wiley and Sons, Inc., New York (1966).
55. Ford, H. W. and Jaffe, S., J. Chem. Phys., 38, 2935 (1963).
56. Kleinman, D. A., Phys. Rev., 125, 87 (1962).
57. Sharma, H., Jervis, R., and Wong, K. Y., J. Phys. Chem., 74, 923 (1970).
58. Douglas, A. E. and Huber, K. P., Can. J. Phys., 43, 74 (1965).
59. Busch, G. and Wilson, K., J. Chem. Phys., 56, 3638 (1972).
60. Gaedtke, H., Hippler, H., and Troe, J., Chem. Phys. Lett., 16, 177 (1972).
61. Herzberg, G., Electronic Spectra of Polyatomic Molecules, Van Nostrand Reinhold Company, New York (1966).
62. Badcock, C. C., Sidebottom, H. W., Calvert, J. G., Rabe, B. R., and Damon, E. K., J. Amer. Chem. Soc., 94, 19 (1972).
63. Verdick, J., Nuc. Appl., 6, 474 (1969).

64. Marsden, M. J. and Bird, G. R., J. Chem. Phys., 59, 2766 (1973).
65. Bird, G. R. and Marsden, M. J., J. Mol. Spect., 50, 403 (1974).

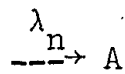
APPENDIX

REFINED DISCUSSION OF THE CONSECUTIVE TWO-PHOTON ABSORPTION PROCESS

The simplified kinetic model adopted for the two-photon absorption process is as follows:



• (deactivating steps)



Here γ_1 and γ_2 are the effective first-order excitation rate constants which are given by

$$\gamma_1 = \int_{-\infty}^{+\infty} I_1(\nu_1) \sigma_1(\nu_1) d\nu_1 \quad (A4)$$

and

$$\gamma_2 = \int_{-\infty}^{+\infty} I_2(\nu_2) \sigma_2(\nu_2) d\nu_2, \quad (A5)$$

where $I_1(\nu_1)$, $I_2(\nu_2)$ are the intensity distributions and $\sigma_1(\nu_1)$, $\sigma_2(\nu_2)$ are the absorption cross sections for the first and second photons, respectively, and the λ_i are the first order or pseudo-first order deactivation rate constants.

The rate equations of interest for the above kinetic scheme are given below:

$$\frac{d(A^*)}{dt} = \gamma_1(A) - [\gamma_2 + \sum_{i=1}^n \lambda_i](A^*) \quad (A6)$$

$$\frac{d(P)}{dt} = \gamma_2(A^*). \quad (A7)$$

The amount of product, P, formed in the process is calculated by solution of equation (A6) for (A*), substitution into equation (A7) and solution of this for (P). The difficulty of solution depends on what type of time dependence one chooses for the γ_1 and γ_2 terms and on the photolysis geometry.

The above equations will be solved analytically for the following set of assumptions:

$$\begin{aligned} (a) \quad \gamma_1(t) &= \gamma_1 & 0 \leq t \leq T \\ &= 0 & t > T \\ \gamma_2(t) &= 0 & 0 \leq t < \tau \\ &= \gamma_2 & \tau \leq t \leq T + \tau \\ &= 0 & t > T + \tau \end{aligned}$$

(This means two square wave pulses of duration, T, separated by a delay time τ),

(b) None of the transitions are saturated and Beers law, in the form of

$$I_x = I_0 \exp[-\sigma n x]$$

where n is the absorber particle density and x is the path length, is valid,

(c) The photolysis geometry is that of a cylindrical cell illuminated by collinear, collimated beams of area A and uniform flux across that area.

Using the above assumptions, the total amount of product formed will be given by

$$(P)_T = \left[\frac{\gamma_1 \gamma_2}{\gamma_2 + \lambda_1} \right] n_a T_{\text{eff}} L_{\text{eff}} A \quad (\text{A8})$$

where n_a = particle density of species a

A = beam area

T_{eff} = effective photolysis time

and L_{eff} = effective photolysis length.

The effective photolysis length is obtained by assuming that I_1 decreases over the cell length following Beer's law, but that I_2 remains essentially constant, and then integrating over the length of the cell, L , to give the result,

$$L_{\text{eff}} = \frac{[1 - \exp(-\sigma_1 n_a L)]}{\sigma_1 n_a} \quad (\text{A9})$$

The effective photolysis time is dependent on the delay time, τ , between pulses, the second excitation rate coefficient, γ_2 , and the deactivation steps (let $\lambda = \sum_{i=1}^n \lambda_i$). The solution gives the final result for T_{eff} of the following:

$$\begin{aligned} T_{\text{eff}} = (T - \tau) &+ \frac{[-(\gamma_2 + \lambda)(T - \tau)]}{(\gamma_2 + \lambda)} + \frac{1}{\lambda} (e^{-\lambda\tau} - 1) (e^{-(\gamma_2 + \lambda)(T - \tau)} - 1) \\ &+ (e^{-(\gamma_2 + \lambda)(T - \tau)} - 1) \left[\frac{1}{(\gamma_2 + \lambda)} (e^{-(\gamma_2 + \lambda)(T - \tau)} - 1) \right. \\ &\left. + \frac{1}{\lambda} (e^{-\lambda\tau} - 1) e^{-(\gamma_2 + \lambda)(T - \tau)} \right]. \end{aligned} \quad (\text{A10})$$

In applying this model to the two-photon dissociation performed in this research, the delay time τ is zero and $I_1 = I_2$. Under these conditions the expression for the total amount of product simplifies to

the following:

$$(P)_T = \frac{\gamma_1 \gamma_2^n L_{\text{eff}}^{\text{AT}}}{(\gamma_2 + \lambda)} \left[1 + \frac{e^{-(\gamma_2 + \lambda)T} - 1}{(\gamma_2 + \lambda)T} \right]. \quad (\text{A11})$$

The more general expression has importance in application to photochemical isotope separation by the two-photon dissociation or ionization processes.

For any given atom or molecule and laser excitation system, many variables become fixed, the pressure of the system and the delay time between pulses remaining the major variables. Optimization of the system may be desired for some reason, possibly economic requirements.

The pressure enters into consideration in the excitation rate which is proportional to pressure, in the effective length term, L_{eff} , and in the deactivation constants, λ . The quenching of the excited state (A^*) can be described by the relation,

$$\frac{d(A^*)}{dt} = \lambda_Q(A^*), \quad (\text{A12})$$

where $\lambda_Q = k_Q(M)$ and (M) is the pressure of the quenching gas and k_Q is the bimolecular quenching constant. If (M) remains essentially constant in time, then λ_Q is a pseudo-first order constant.

The fact that the excited state has a finite lifetime and that the pulses have a finite duration places the optimal delay time somewhere between the start ($t = 0$) and end ($t = T$) of the first exciting pulse.

Choosing some typical values for the constants involved (see Table A1) the product formed has been evaluated as a function of delay time for seven different pressures (see Figure A1). The absorber is taken to be an isotopic species with an abundance of ~1%, so the

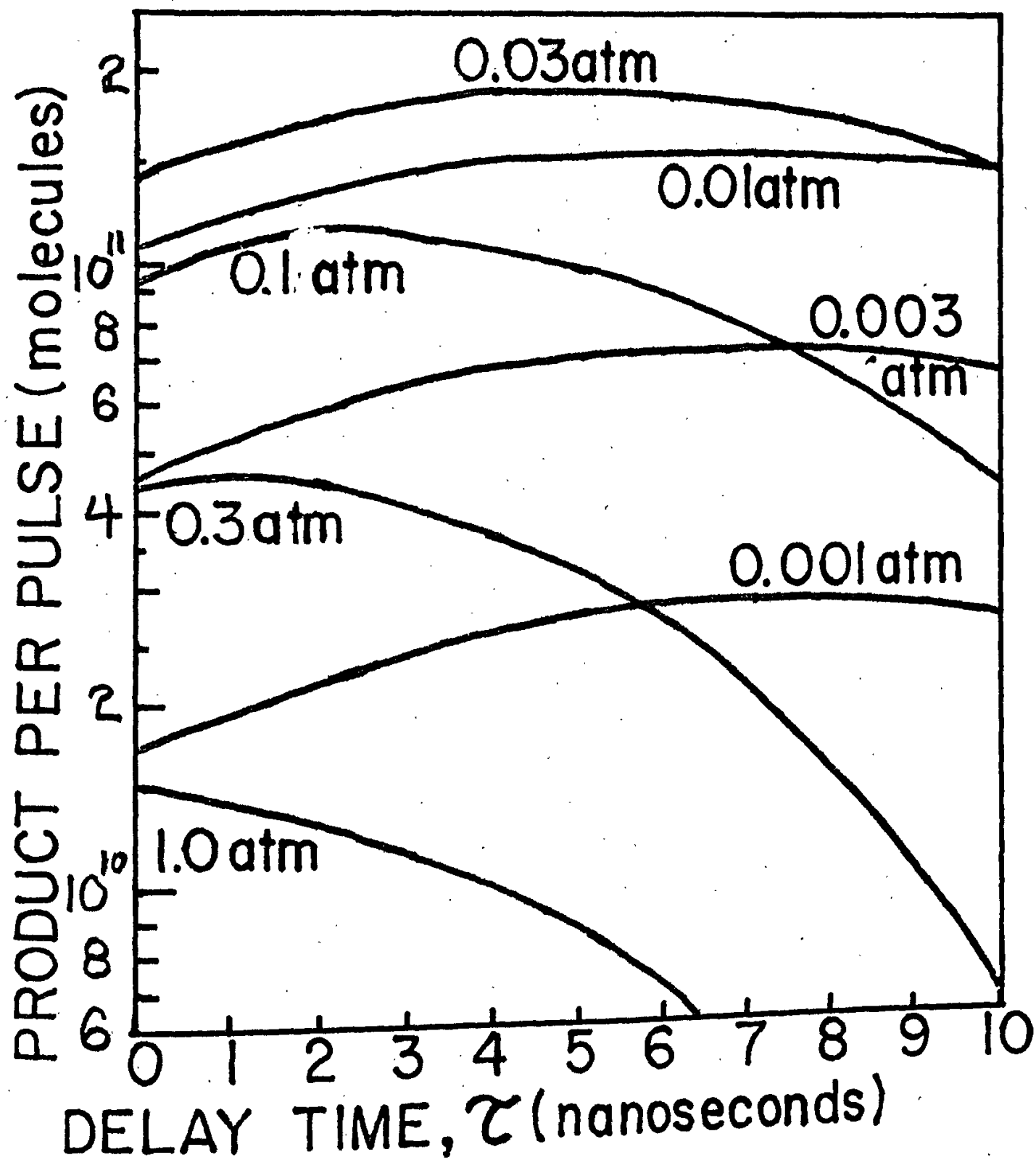
Table A1

Definition of Terms*

I_1	=	peak laser intensity 1	=	1.0×10^{22}	photons/cm ² -sec
I_2	=	peak laser intensity 2	=	1.0×10^{24}	photons/cm ² -sec
σ_1	=	cross section 1	=	4×10^{-18}	cm ² /molecule
σ_2	=	cross section 2	=	4×10^{-18}	cm ² /molecule
L	=	path length	=	100	cm
τ_0	=	radiative lifetime	=	3.0×10^{-8}	sec
k_Q	=	quenching constant	=	1.0×10^{-10}	cm ³ /part-sec
α	=	isotopic abundance	=	0.01	
T	=	pulse width	=	1.0×10^{-8}	sec
n_1	=	particle density of A molecules	=	2.5×10^{19}	part/cm ³ -atm
τ	=	delay time between pulses			
A	=	beam area	=	0.1	cm ²
γ_1	=	$I_1 \sigma_1$ (first absorption rate)	=	4×10^4	sec ⁻¹
γ_2	=	$I_2 \sigma_2$ (second absorption rate)	=	4×10^6	sec ⁻¹
λ_1	=	$(\frac{1}{\tau_0} + k_Q n_1)$	=		sec ⁻¹ (deactivation rate)
n'_1	=	isotope particle density	=	αn_1	

* Including assumed parameter values for calculations giving results presented in diagram.

Figure A1 Calculated Product per Laser Pulse Versus Delay Time for
a Series of Absorber Pressures



absorber density and quencher density will differ by a factor of ~ 100 .

From the graph of these results one can observe qualitatively the following trends;

(1) Neglecting delay time; a maximum of product is obtained at intermediate pressures, and pressure considerations dominate over delay time,

(2) The optimum delay time goes to zero for high pressures and tends towards the width of the pulse (~ 10 nanoseconds) at low pressures. At the intermediate pressures where product optimization due to pressure considerations occurs, the delay time for optimal product formation lies between these two limits.

The optimizations of pressure and delay time will vary from system to system and must be calculated for each specific one chosen. However, these considerations point out the necessity of careful evaluation of all parameters in designing a separation scheme for the greatest efficiency, particularly if it is intended to use the process for economic reasons.